Electronic Supplementary Material (ESI) for Dalton Transactions.
This journal is © The Royal Society of Chemistry 2014

Electronic Supplementary Information

Binding of Copper(II) Polypyridyl Complexes to DNA and Consequences for DNA-based Asymmetric Catalysis

Apparao Draksharapu, Arnold J. Boersma, Miriam Leising, Auke Meetsma, Wesley R. Browne and Gerard Roelfes

Contents

Electronic Supplementary Information 1

Binding of Copper(II) Polypyridyl Complexes to DNA and Consequences for DNA-based Asymmetric Catalysis 1

1. Synthesis and characterization 2

2. Structure determination by X-ray crystallography 3

3. Experimental section 5

4. ^{1}H NMR spectroscopy 7

5. FTIR spectroscopy 8

6. Raman spectroscopy 14

7. EPR spectroscopy at 77 K 27

8. Room temperature EPR spectroscopy 29

9. Effect of ionic strength 30

10. Sequence dependent EPR spectroscopy 31

11. UV/Vis absorption spectroscopy 32

12. Interaction of Cu-L with st-DNA (Raman and resonance Raman spectroscopy) 34

13. Effect of salts on the Raman, EPR and UV/Vis absorption spectroscopy of 1 and 5 35

14. Circular Dichroism 38

14. Linear Dichroism 39

15. Viscosity 41

References 41

1. Synthesis and characterization

[D8]-bpy and [D8]-phen were prepared according to literature methods.[1] [Cu([D8]-bpy)$(NO_3)_2$] (**2a**) was generated in situ by adding equimolar aqueous solutions of [D8]-bpy and $Cu(NO_3)_2 \cdot 3H_2O$ for Raman experiments. [Cu([D8]-phen)$(NO_3)_2$] (**3a**) was generated in situ by adding equimolar aqueous solutions of [D8]-phen and $Cu(NO_3)_2 \cdot 3H_2O$ for Raman experiments.

[D_{12}]-dmbpy. 1 g of dmbpy was added to mixture of D_2O (18 mL) and NaOD (2 mL, 1 M in D_2O). The resulting solution was transferred into a Teflon lined pressure vessel (Parr Instrument company) and heated at 200 ºC for one week. The solution was allowed to cool and the product extracted with dichloromethane and solvent removed in vacuo. [D_{12}]-dmbpy was obtained as white solid. An average extent of 89.5% deuteration was achieved by ^{1}H NMR spectroscopy (Fig. S1).[1]

[Cu(dmbpy)$(NO_3)_2$] (1). 4,4'-dimethylbipyridine (73.4 mg, 0.4 mmol) in 7.5 mL ethanol was added to $Cu(NO_3)_2 \cdot 3H_2O$ (193.1 mg, 0.8 mmol) in 2.5 mL of ethanol. The blue solution obtained was placed in an ethyl acetate bath. After 2 d, [Cu(dmbpy)$(NO_3)_2$] (**1**) was recovered as blue crystals, which were suitable for analysis by X-ray crystallography. Yield: 132 mg, 0.355 mmol, 88%. Anal. Calcd for $C_{12}H_{12}CuN_4O_6$: C, 38.77 H, 3.25 N, 15.07. Found: C, 38.38 H, 3.22 N, 14.88.

[Cu([D_{12}]-dmbpy)$(NO_3)_2$] (1a). [D_{12}]-4,4'-dimethylbipyridine (71.6 mg, 0.36 mmol) in 10 mL of ethanol was added to $Cu(NO_3)_2 \cdot 3H_2O$ (88.18 mg, 0.36 mmol) in 10 mL of ethanol. The blue solution obtained was placed in an ethyl acetate bath. After 2 d, [Cu([D_{12}]-dmbpy)$(NO_3)_2$] (**1a**) was recovered as blue crystals. Yield: 94 mg, 0.24 mmol, 67%.

[Cu(terpy)$(NO_3)_2$] $\cdot H_2O$ (4). Terpyridine (100.4 mg, 0.43 mmol) in 2 mL of ethanol was added with stirring to $Cu(NO_3)_2 \cdot 3H_2O$ (104.5 mg, 0.433 mmol) in 2 mL of ethanol. The resulting solution was stirred for 2 h. [Cu(terpy)$(NO_3)_2] \cdot H_2O$ (**4**) was isolated as a green powder by filtration and washed with a minimum amount of ethanol and ethyl acetate. Yield: 160 mg, 0.36 mmol, 85%. Anal. Calcd for $C_{15}H_{13}CuN_5O_7$: C, 41.05 H, 2.99 N, 15.96. Found: C, 41.36 H, 2.81 N, 16.06.

2a and **3a** were prepared in situ by adding aqueous solution of Cu(II) to the corresponding deuterated ligand in the solid state.

2. Structure determination by X-ray crystallography

Blue-colored crystals of **1** were obtained from ethanol by saturation with ethyl acetate. A platelet-shaped crystal with the dimensions of 0.37 x 0.33 x 0.04 mm was mounted on top of a glass fiber, and aligned on a *Bruker SMART APEX CCD* diffractometer (Platform with full three-circle goniometer). The diffractometer was equipped with a 4K *CCD* detector set 60.0 mm from the crystal. The crystal was cooled to 100(1) K using the *Bruker KRYOFLEX* low-temperature device. Intensity measurements were performed using graphite monochromated Mo-K$\bar{\alpha}$ radiation from a sealed ceramic diffraction tube (*SIEMENS*). Generator settings were 50 KV/ 40 mA. *SMART* was used for preliminary determination of the unit cell constants and data collection control. The intensities of reflections of a hemisphere were collected by a combination of 3 sets of exposures (frames). Each set had a different ϕ angle for the crystal and each exposure covered a range of 0.3° in ω. A total of 1800 frames were collected with an exposure time of 10.0 seconds per frame. The overall data collection time was 8.0 h. Data integration and global cell refinement was performed with the program *SAINT*. The final unit cell was obtained from the *xyz* centroids of 5744 reflections after integration. Intensity data were corrected for Lorentz and polarization effects, scale variation, for decay and absorption: a multi-scan absorption correction was applied, based on the intensities of symmetry-related reflections measured at different angular settings (*SADABS*), and reduced to F_o^2. The program suite *SAINTPLUS* was used for space group determination (*XPREP*). The structure was solved by Patterson methods and extension of the model was accomplished by direct methods applied to difference structure factors using the program *DIRDIF*. The positional and anisotropic displacement parameters for the non-hydrogen atoms were refined. A subsequent difference Fourier synthesis resulted in the location of all the hydrogen atoms, which coordinates and isotropic displacement parameters were refined.[a]

All refinement calculations and graphics were performed on a HP XW6200 (Intel XEON 3.2 GHz) / Debian-Linux computer at the University of Groningen with the program packages *SHELXL* (least-square refinements), a locally modified version of the program *PLUTO* (preparation of illustrations) and *PLATON* package (checking the final results for missed symmetry with the *MISSYM* option, solvent accessible voids with the *SOLV* option, calculation of geometric data and the *ORTEP* illustrations).

a. Beurskens, P.T., Beurskens, G., Gelder, R. de, García-Granda, S., Gould, R.O., Israël, R. & Smits, J.M.M. (1999). The *DIRDIF*-99 program system, Crystallography Laboratory, University of Nijmegen, The Netherlands

Table S 1 Crystal data and details of the structure determination.

Chemical Formula	$C_{12}H_{12}CuN_4O_6$
Molecular Weight, g.mol^{-1}	371.80
Crystal system	monoclinic
Space group, no	$P2_1/n$, 14
a, Å	11.4772(8)
b, Å	8.7255(6)
c, Å α, deg	15.469(1) 90
β, deg γ, deg	107.041(1) 90
V, Å^3	1481.12(17)
Θ range unit cell: min.-max., deg; reflections	2.62 - 29.45 ; 5744
Formula_*Z*	4
SpaceGroup_*Z*	4
Z' (= Formula_Z / SpaceGroup_*Z)*	1
ρ_{calc}, g.cm^{-3}	1.667
F(000), electrons	756
μ(Mo K$\bar{\alpha}$), cm^{-1}	15.12
Colour, habit	blue, platelet
Approx. crystal dimension, mm	0.37 x 0.33 x 0.04
Number of reflections	3665
Number of refined parameters	256
Final agreement factors:	
$wR(F^2) = [\sum [w(F_o^2 - F_c^2)^2] / \sum [w(F_o^2)^2]]^{1/2}$	0.0758
Weighting scheme: *a, b* $w = 1/[\sigma^2(F_o^2) + (aP)^2 + bP]$ And $P = [\max(F_o^2,0) + 2F_c^2] / 3$	0.0381, 0.8004
$R(F) = \sum (\|F_o\| - \|F_c\|) / \sum \|F_o\|$ For $F_o > 4.0\ \sigma(F_o)$	0.0298
GooF = S = $[\sum [w(F_o^2 - F_c^2)^2] / (n-p)]^{½}$ n = number of reflections p = number of parameters refined	1.041
Residual electron density in final Difference Fourier map, e/Å^3	 -0.27, 0.53(8)

3. Experimental section

Physical Methods

Elemental analyses were performed with a Foss-Heraeus CHN Rapid or a EuroVector Euro EA elemental analyser. FTIR spectra were recorded using a UATR (ZnSe) equipped Perkin Elmer Spectrum400 FTIR spectrometer with a liquid nitrogen cooled MCT detector. Details of X-Ray structural analysis and Raman spectroscopy[2] see ESI. EPR spectra were recorded on a Bruker ECS 106 spectrometer, equipped with a Bruker ECS 041 XK microwave bridge and a Bruker ECS 080 magnet. The samples were prepared 2 h in advance and stored on ice. The samples were added to EPR tubes and flash frozen to 77 K. The EPR spectra were baseline corrected by subtraction of the spectrum of 20 mM mops buffer pH 6.5, 1.8 vol% DMSO, recorded under identical conditions. Among the co-solvents tested, DMSO improved the glass quality most. The spectra obtained were simulated using the programs SimFonia (Bruker) and Winsim. UV/Vis absorption spectra were recorded with a Specord600 (AnalytikJena) spectrophotometer in 1 cm path length quartz cuvettes. LD and CD spectra were recorded on a Jasco J-815 Circular Dichroism spectrophotometer. For LD, samples were aligned using a micro-Couette cell from Kromatek,[3] with an applied rotation speed of 3000 rpm for st-DNA. Raman spectra were obtained in an ca. 155° backscattering arrangement with excitation at 244 nm (5 mW at sample) and 266 nm (8 mW at sample) obtained by frequency doubling 488 nm and 532 nm respectively using a WaveTrain (Coherent), at 355 nm (10 mW, Cobolt Lasers) and 473 nm (100 mW, Cobolt Lasers). Raman scattering was collected and collimated (f = 7.5 cm) and subsequently refocused (f = 17.5 cm, or 7.5 cm in the case of 473 nm) via a pair of 2.5 cm diameter plano-convex lens. The collected light was filtered by an appropriate long pass edge filter (Semrock) and dispersed by a Shamrock300i (at 473 nm) or 500i spectrograph (Andor Technology) with a 1200 l/mm grating blazed at 500 nm, or 2400 l/mm blazed at 300 nm and acquired with a DV420A-BU2 CCD camera (Andor Technology). The slit width was set to 10 or 20 µm. Data were recorded and processed using Solis (Andor Technology), Spekwin32[4] and Spectrum (Perkin Elmer) with spectral calibration performed using the Raman spectrum of cyclohexane or acetonitrile/toluene 50:50 (v:v).[5] Samples were held in 10 mm path length quartz cuvettes. Solvent subtraction and a multipoint baseline correction were performed for all spectra. Raman spectra were recorded at λ_{exc} 785 nm using a Perkin Elmer Raman Station at room temperature. KCl dispersed Cu complexes were prepared by crushing the desired Cu complex with KCl in a mortar.

Viscometry was performed using an Ostwald viscometer thermostated at 22 °C. A solution containing 2 mg/mL st-DNA in 20 mM MOPS buffer pH 6.5 was sonicated for 30 min, cooled at 4 °C for 10 min, and sonicated for a further 30 min. The solution was filtered over a 0.45 µm filter, and diluted to 0.2 mM in st-DNA base pairs. 6 mL were introduced into the viscometer. The complexes (2 mM in DMSO) were added with 15 µL increments. After addition of the complexes, the solution was mixed by passing air through the tube. After equilibration for 15 min, the flow time was measured four times. The relative viscosity η was obtained from the flow

time t of the st-DNA containing solution with the Cu(II) complex and the flow time t_0 of the solution containing st-DNA alone:

$$\eta = \frac{t - t_0}{t_0}$$

The apparent st-DNA fragment length L/L_0 was calculated from;[6]

$$\left(\frac{\eta}{n_0}\right)^{1/3} = \frac{L}{L_0}$$

The viscosity was corrected for increase due to the addition of DMSO by subtraction (using data obtained with only DMSO added), and plotted versus the Cu(II) complex to DNA base pairs ratio r. The amount of complex bound to DNA was corrected for its binding affinity for st-DNA, which was determined earlier.[**Error! Bookmark not defined.**7] Solution viscosity was found to not change upon addition of the groove-binding agent Hoechst 33258 as expected.

4. ^{1}H NMR spectroscopy

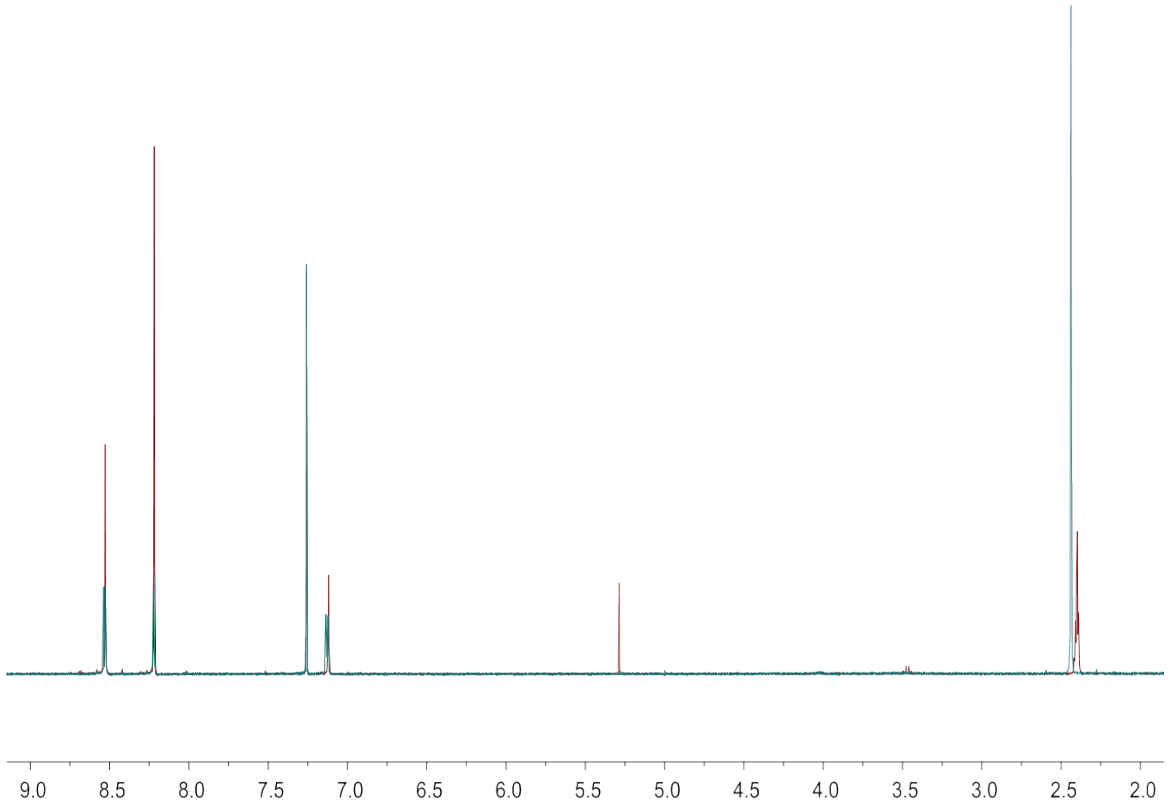

Fig. S 1 ^{1}H NMR (400 MHz) spectra of [H_{12}]-dmbpy (brown) and [D_{12}]-dmbpy (blue) in $CDCl_3$. ^{1}H NMR spectra (400 MHz) were recorded on a Varian Mercury Plus. Chemical shifts are denoted relative to the residual solvent peak ($CDCl_3$, 7.26 ppm).[8]

5. FTIR spectroscopy

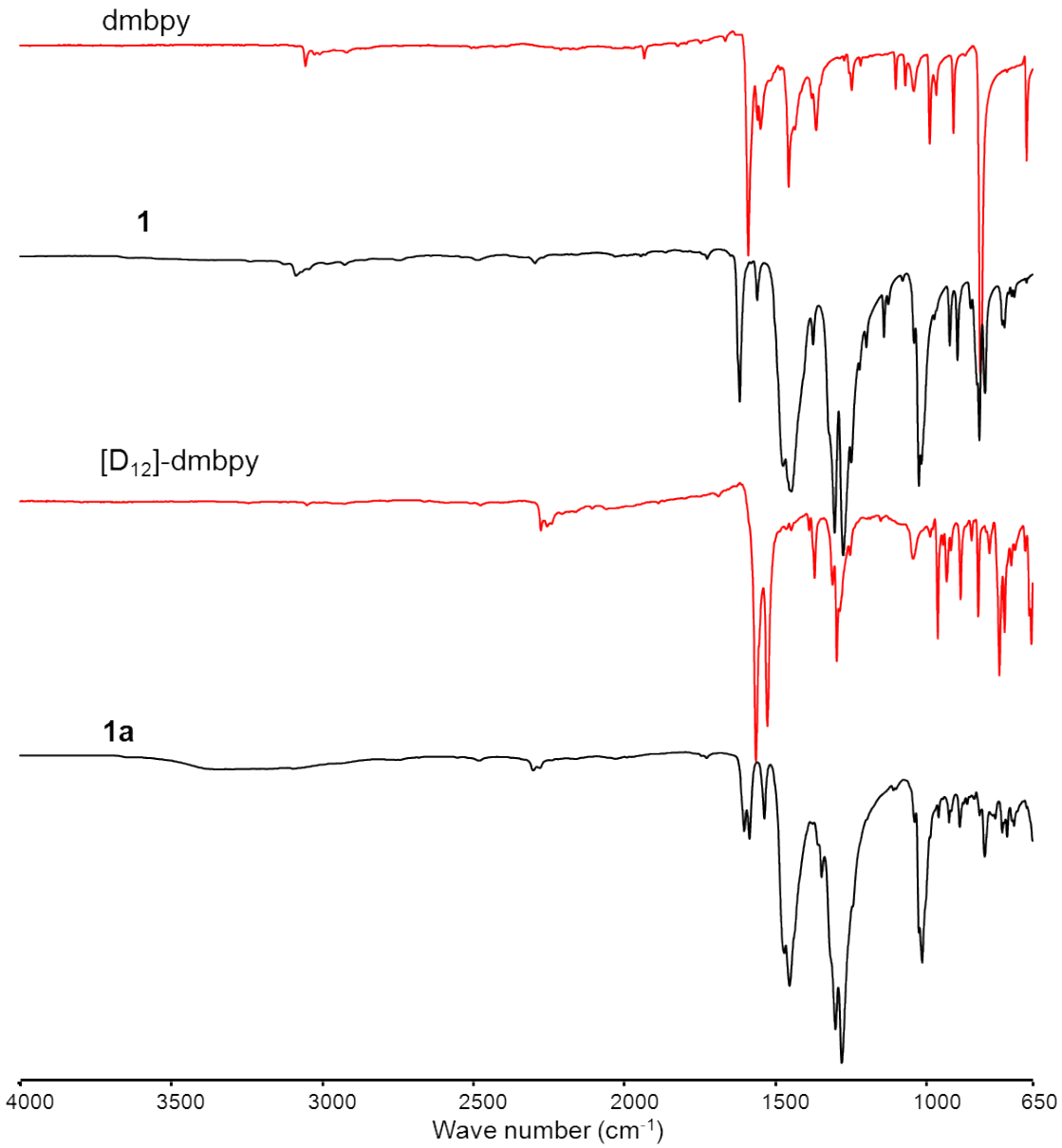

Fig. S 2 ATR-FTIR spectra of $[H_{12}]$-dmbpy and $[D_{12}]$-dmbpy and their Cu(II) complexes **1** and **1a**, respectively.

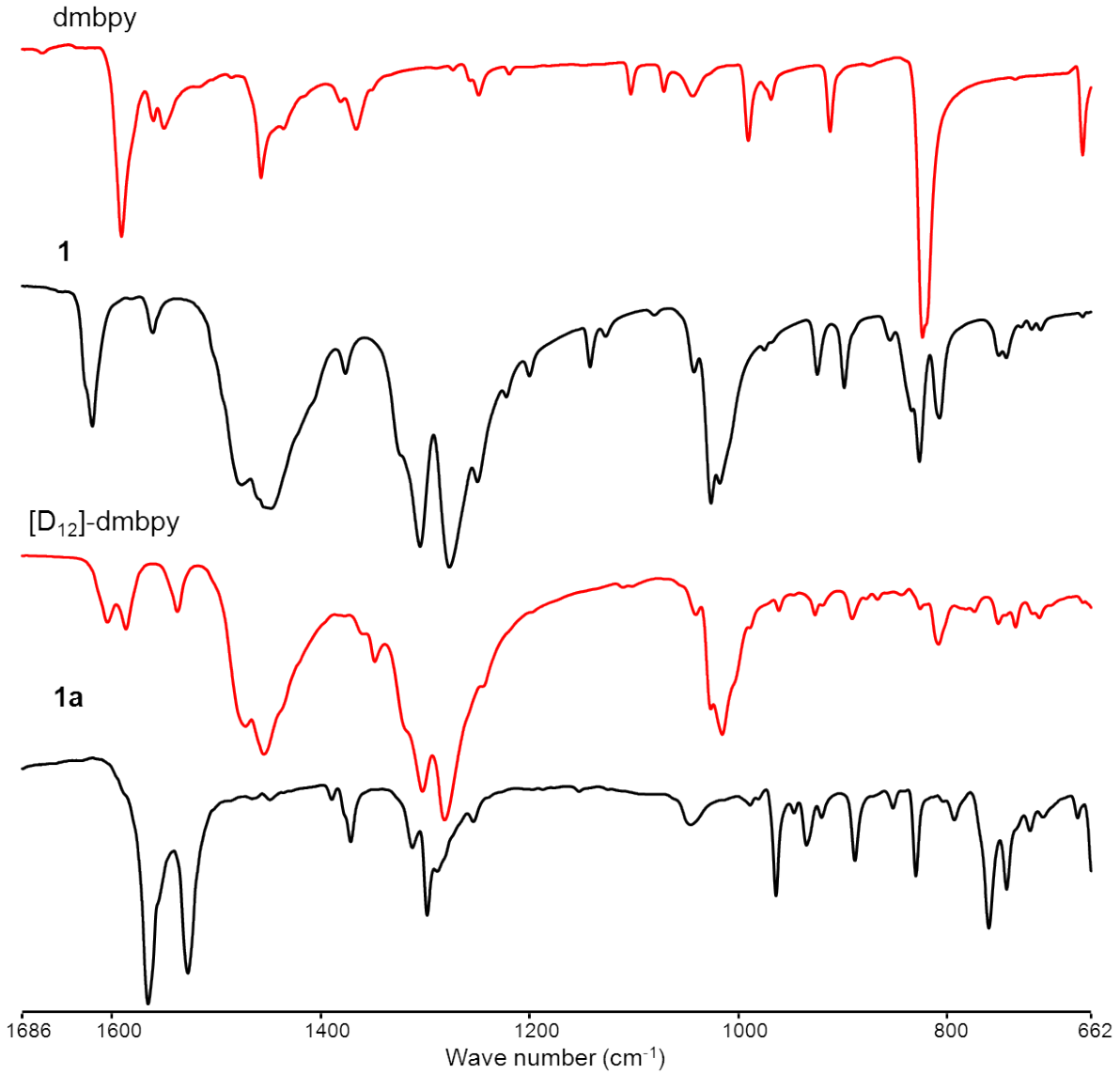

Fig. S 3 ATR-FTIR spectra of $[H_{12}]$-dmbpy and $[D_{12}]$-dmbpy and their Cu(II) complexes **1** and **1a**, respectively.

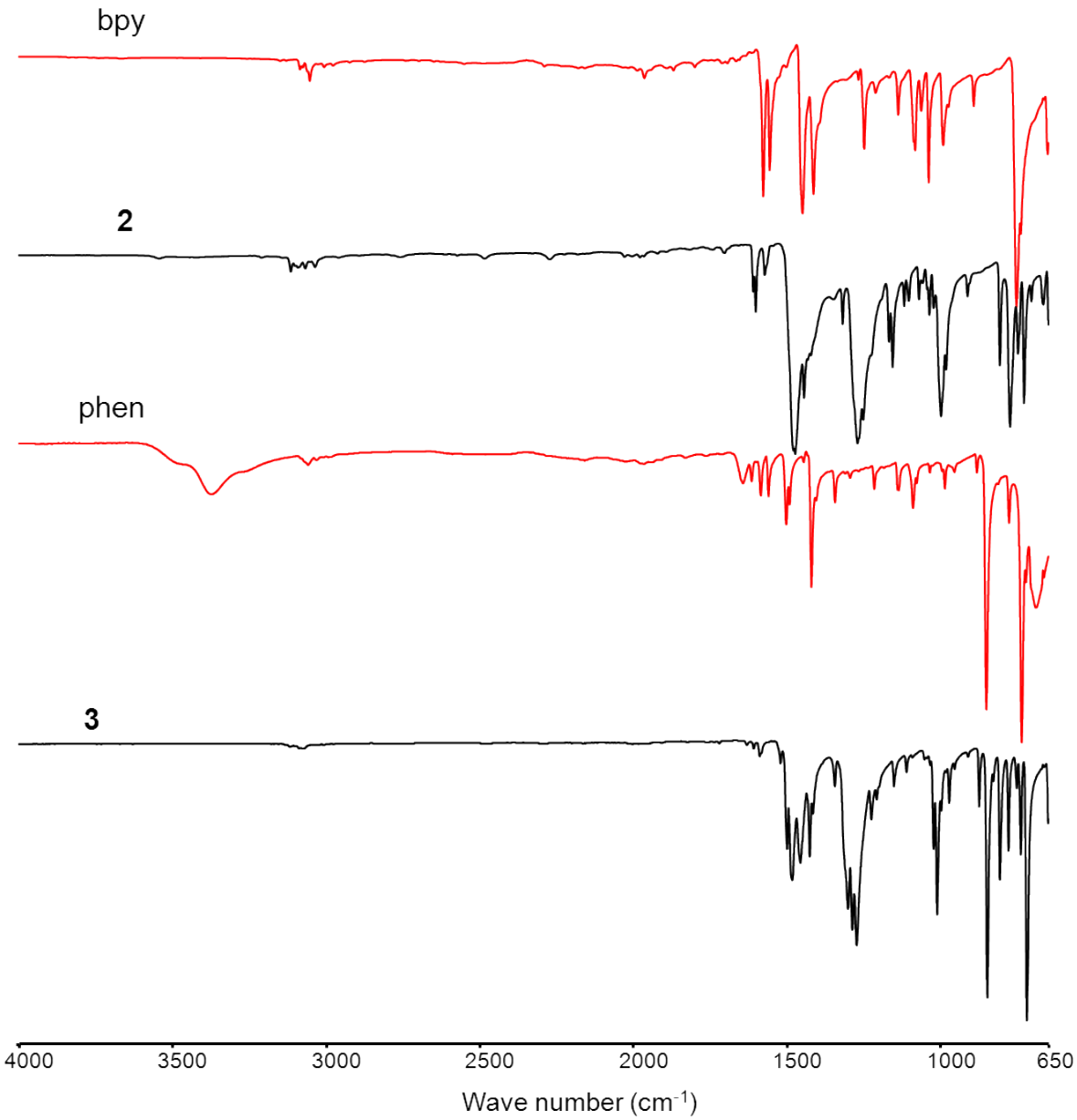

Fig. S 4 ATR-FTIR spectra of bpy and phen and their Cu(II) complexes **2** and **3**, respectively.

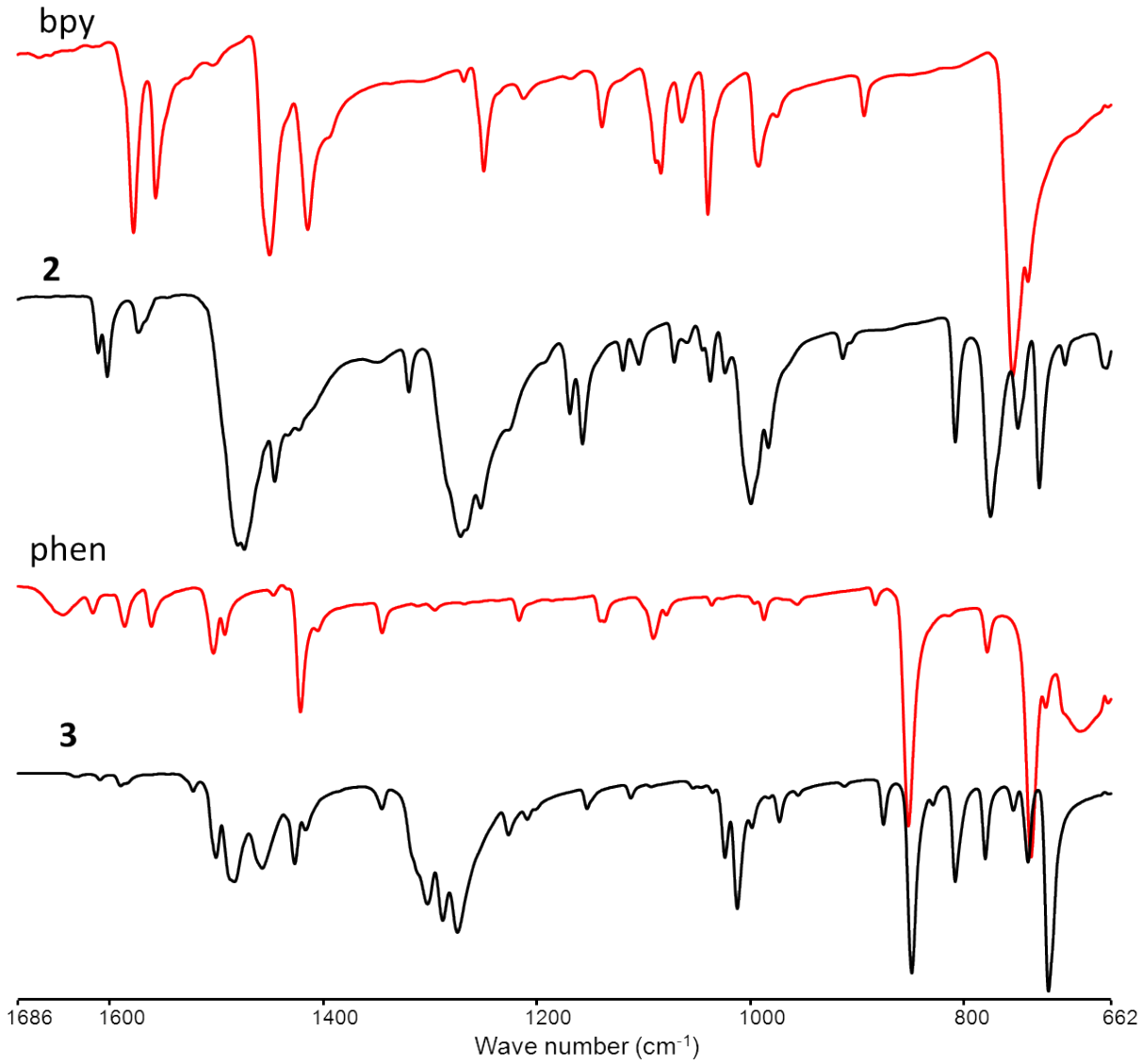

Fig. S 5 ATR-FTIR spectra of bpy and phen and their Cu(II) complexes **2** and **3**, respectively.

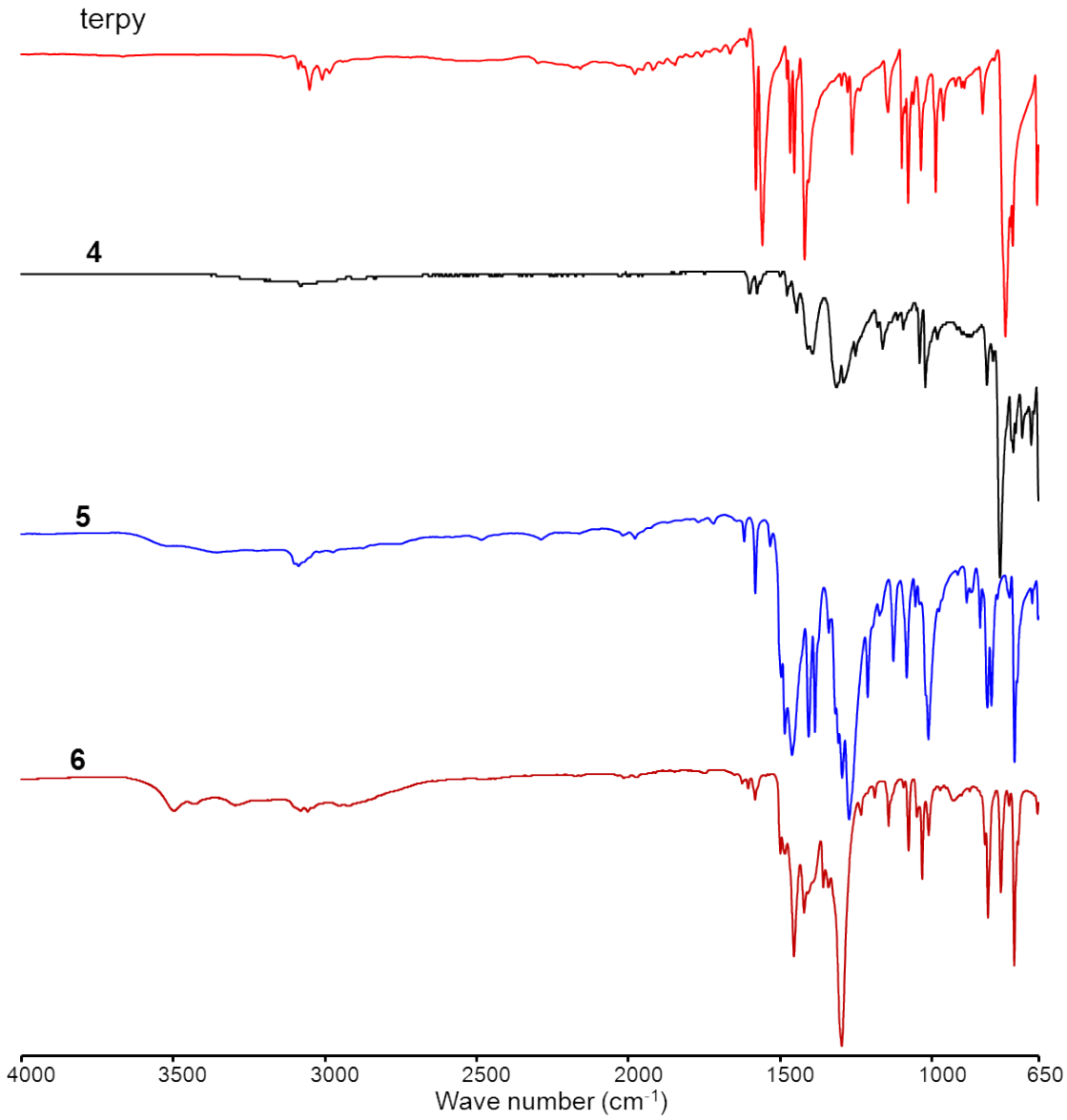

Fig. S 6 ATR-FTIR spectra of terpy the complexes **4**, **5** and **6**.

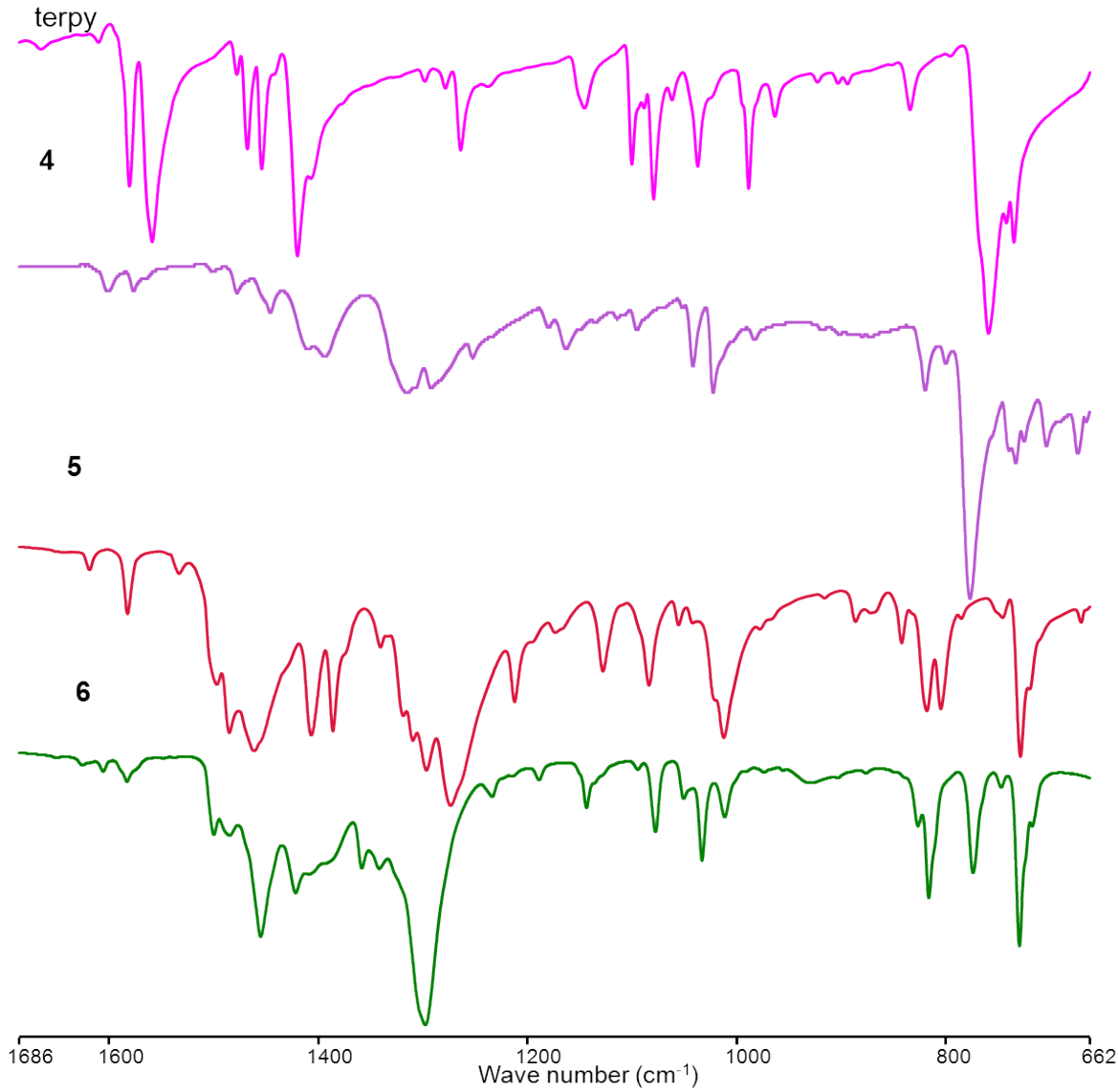

Fig. S 7 ATR-FTIR spectra of terpy the complexes **4**, **5** and **6**.

6. Raman spectroscopy

Wavelength-dependent Raman and resonance Raman spectroscopy of st-DNA

The non-resonant Raman spectra of st-DNA was obtained at λ_{exc} 473 nm in solution and at 785 nm in the solid state. Although the Raman spectrum obtained at 473 nm shows a poor signal to noise ratio, the close correspondence with the Raman spectrum of a solid sample of st-DNA is apparent. St-DNA shows absorption between 230 and 300 nm, and hence resonance enhancement of the Raman spectrum of st-DNA is observed at λ_{exc} 244 and 266 nm, with (pre)resonance enhancement at 355 nm (Fig. S 8).

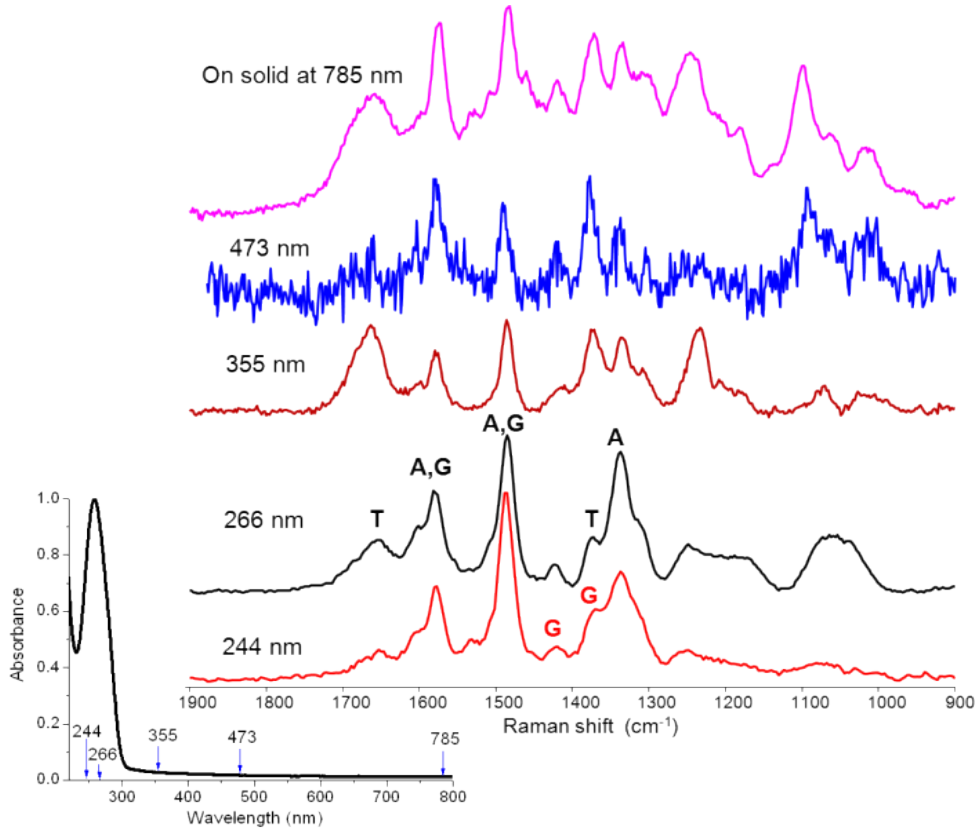

Fig. S 8 Wavelength dependent resonance, pre-resonance and non-resonant Raman spectra of st-DNA in MOPS buffer at pH 6.5. UV/Vis absorption and Raman spectra of st-DNA were obtained at 1.3 mg/mL in 20 mM MOPS buffer at pH 6.5. Raman Spectra were solvent subtracted followed by a multipoint baseline correction.

The UV Raman spectra of st-DNA in MOPS buffer were assigned by comparison with earlier assignments for calf-thymus and short stranded DNA.[9] The Raman spectra of st-DNA obtained at λ_{exc} 355 nm, 473 and 785 nm show bands assignable to the carbonyl and aromatic moieties of the nucleotides. Raman spectra obtained at λ_{exc} 355 and 473 nm are similar to the solid state spectrum of st-DNA obtained at λ_{exc} 785 nm. Although the absorptivity of DNA at λ_{exc} 355 nm is low, the Raman spectrum recorded at that wavelength shows enhancement in intensity compared with that at λ_{exc} 473 nm, in particular bands assignable to carbonyl stretching modes are

enhanced to a greater extent with respect to other modes. At λ_{exc} 244 and 266 nm bands associated with purine modes are enhanced most. Resonance enhancement of adenine (A) bands is most pronounced at λ_{exc} 266 nm and guanine (G) bands at λ_{exc} 244 nm.[10] Bands assignable to guanine and adenine overlap at 1600, 1580 and 1484 cm^{-1} at both λ_{exc} 244 and 266 nm. The bands are at 1506, 1421, 1336, 1312 cm^{-1} are assigned to the adenine modes.[9a] The shoulder at 1319 cm^{-1} in the spectrum at λ_{exc} 244 nm is assigned to guanine. The bands at 1654 and 1373 cm^{-1} are assigned to the thymidine. The broad band at 1654 cm^{-1} has been assigned previously as being predominantly a thymidine carbonyl mode and is stronger at λ_{exc} 266 nm.[9a,10]

Raman spectroscopy of complexes 1 – 4

The Raman spectra of **1** - **4** in solution were acquired at λ_{exc} 244, 266, 355 and 473 nm in aqueous solution and at 785 nm both in solution and in the solid state (see below) and show the expected bands at (for **1**) 1621, 1565, 1500, 1427, 1321, 1200 and 1041 cm^{-1}, (for **2**) 1607, 1572, 1501, 1441, 1323, 1177 and 1038 cm^{-1} and (for **4**) 1615, 1602, 1572, 1503, 1479, 1410, 1337, 1299, 1259, 1116, 1044 and 1015 cm^{-1}, which are typical of pyridyl based ligands, and (for **3**) at 1634, 1613, 1592, 1526, 1461, 1436, 1314 and 1058 cm^{-1} (Fig. S 17-22).[2] The expected isotopic shifts were observed for the corresponding isotopologs **1a** - **3a**.

The structure of **1** in the solid state (*vide supra*) and the structure adopted in solution were compared using FTIR and Raman spectroscopy. The FTIR spectrum of **1** in the solid state shows that the pyridine bands at 1590 cm^{-1} were shifted by 27 cm^{-1} to higher wavenumbers compared to the ligand dmbpy.[11] In addition the FTIR spectrum of **1** in the solid state shows strong absorptions at 1013, 1268, and 1440 cm^{-1} assigned to coordinated nitrate.[12] Absorption from unbound NO_3^- at 1362 cm^{-1} was not observed. Similarly, the solid state non-resonant Raman spectra of **1** shows a 14 cm^{-1} shift to higher wavenumber in the pyridyl mode of dmbpy at 1602 cm^{-1} (Fig. S 9).

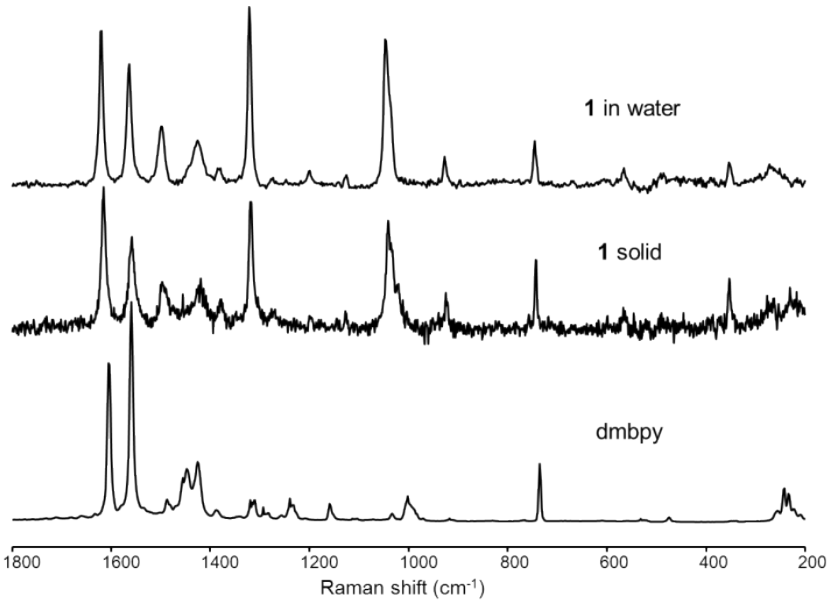

Fig. S 9 Raman spectra of **1** in water (> 50 mM) and in the solid state at λ_{exc} 785 nm. The solid state Raman spectrum of dmbpy is shown for comparison. The Raman spectrum in water is solvent subtracted and a multipoint baseline correction has been applied.

In water at high concentrations (> 50 mM), the Raman spectrum of **1** showed minor changes to that observed in the solid state with all bands undergoing a shift to higher wavenumbers (~6 cm^{-1}). The shifts suggest exchange of the nitrate ligands for aquo ligands, which is expected in view of nitrate's low association constant to copper of 0.07 ± 0.02 M^{-1} in water.[13] Similar changes were observed for complexes **2**, **3** and **4** also (Fig. S 10-13). Overall, vibrational spectroscopy suggests that the structure of **1** does not change significantly upon dissolution in water, except for the displacement of the coordinated nitrate ions by water.

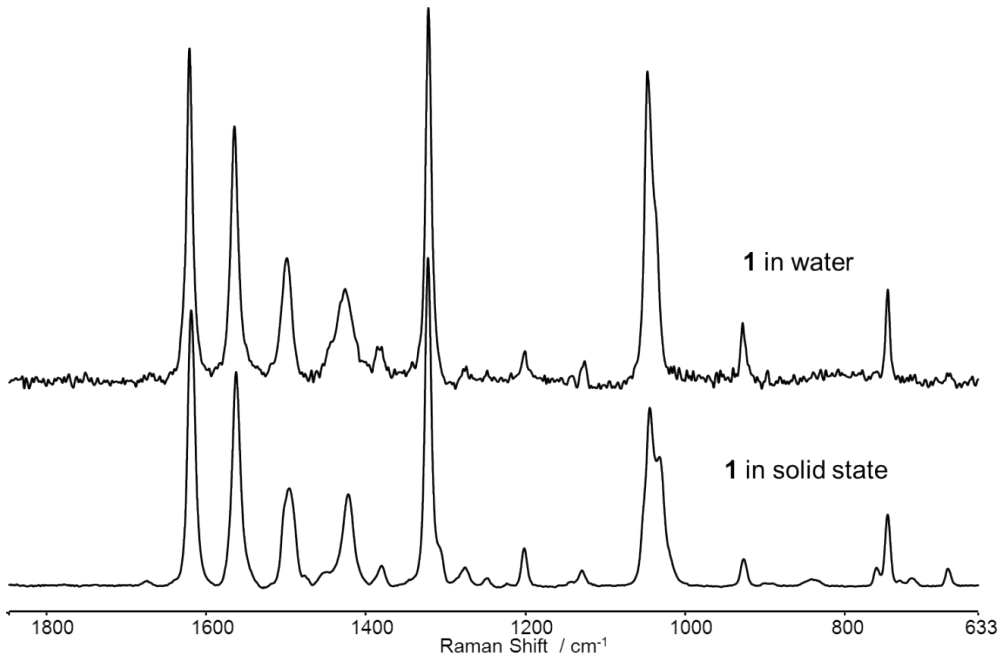

Fig. S 10 Raman spectra of **1** in water (λ_{exc} 785 nm) and as a dispersion in KCl (at λ_{exc} 473 nm, line focused sampling). Raman spectra were KCl background subtracted followed by a multipoint baseline correction.

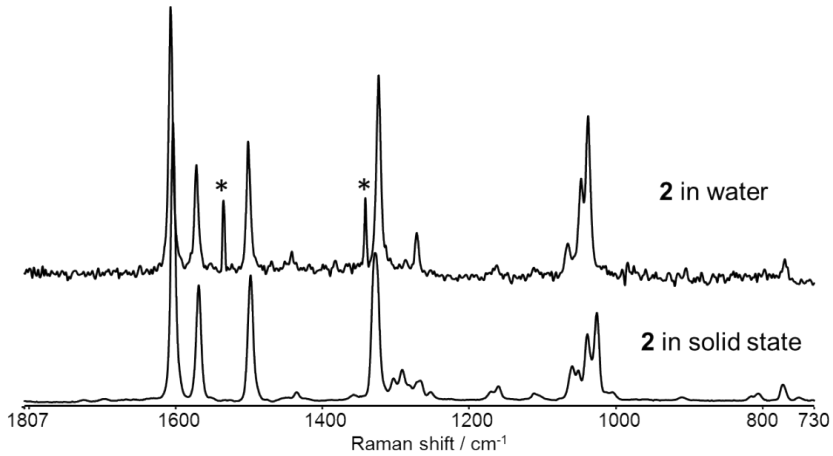

Fig. S 11 Raman spectra of **2** in water (at λ_{exc} 785 nm) and dispersed in solid KCl (at λ_{exc} 473 nm, line focused sampling). Raman spectra were solvent and KCl background subtracted, respectively, followed by a multipoint baseline correction. *cosmic signals.

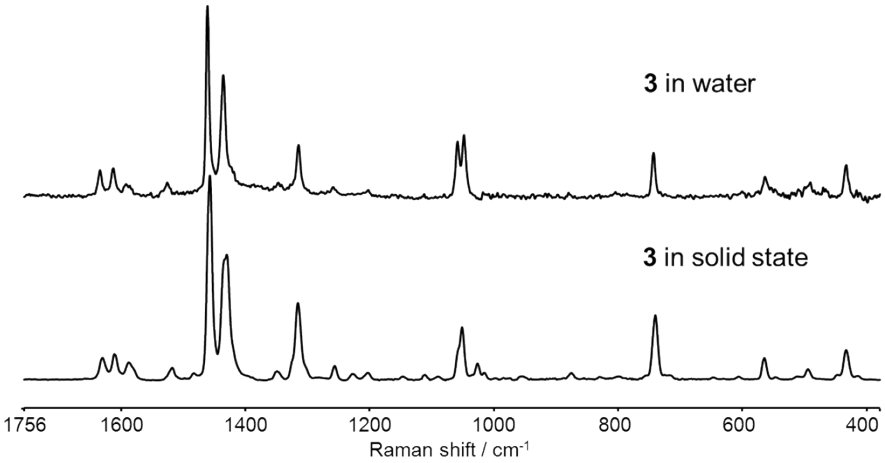

Fig. S 12 Raman spectra of **2** in water (at λ_{exc} 785 nm) and dispersed in solid KCl (at λ_{exc} 473 nm, line focused). Raman spectra were solvent and KCl background subtracted, respectively, followed by a multipoint baseline correction.

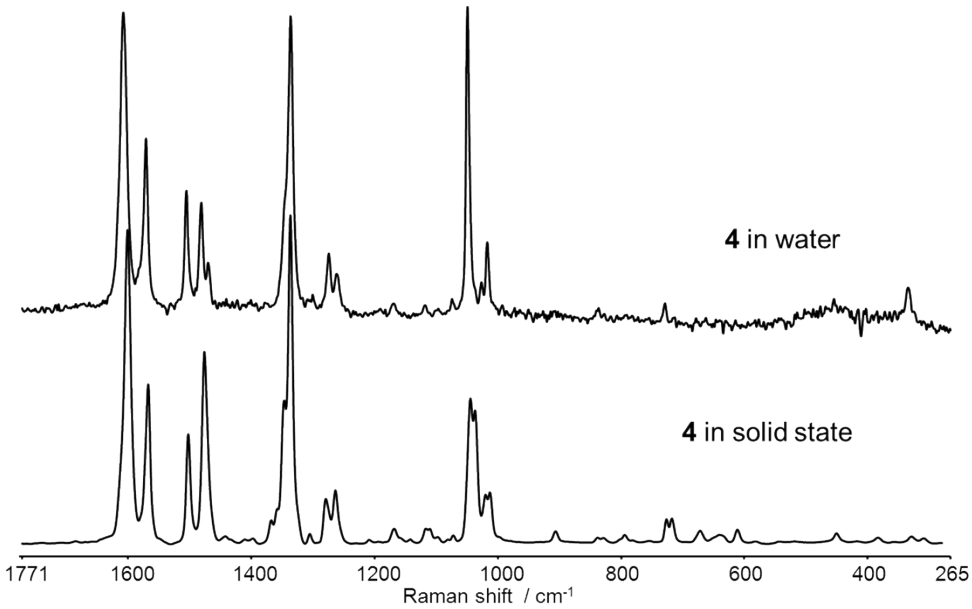

Fig. S 13 Raman spectra of **4** in water (at λ_{exc} 785 nm) and dispersed in KCl (at λ_{exc} 473 nm, line focused). Raman spectra were solvent and KCl background subtracted, respectively, followed by a multipoint baseline correction.

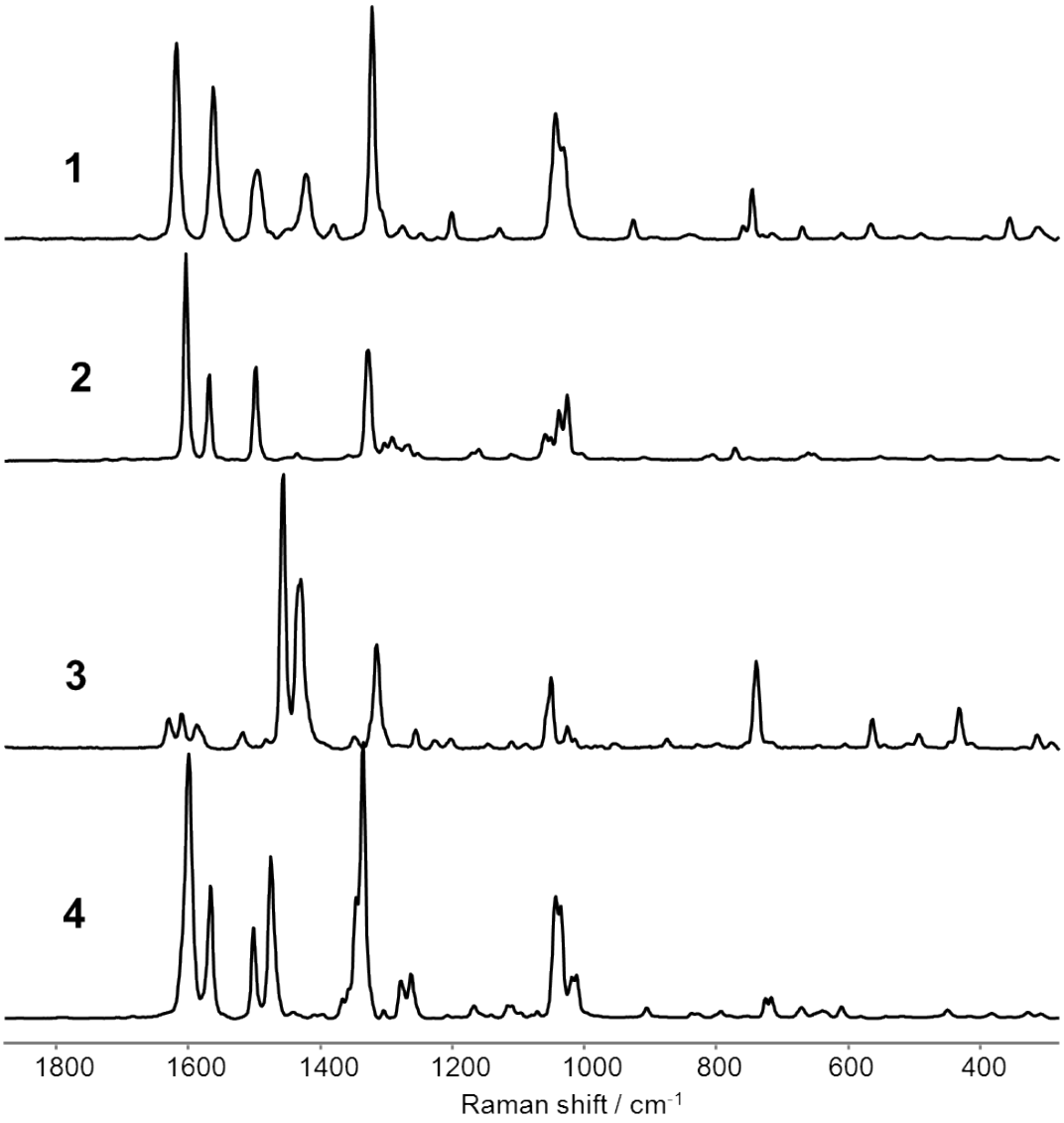

Fig. S 14 Raman spectra of **1** - **4** dispersed in KCl at λ_{exc} 473 nm (line focused sampling). Raman spectra were KCl background subtracted followed by a multipoint baseline correction.

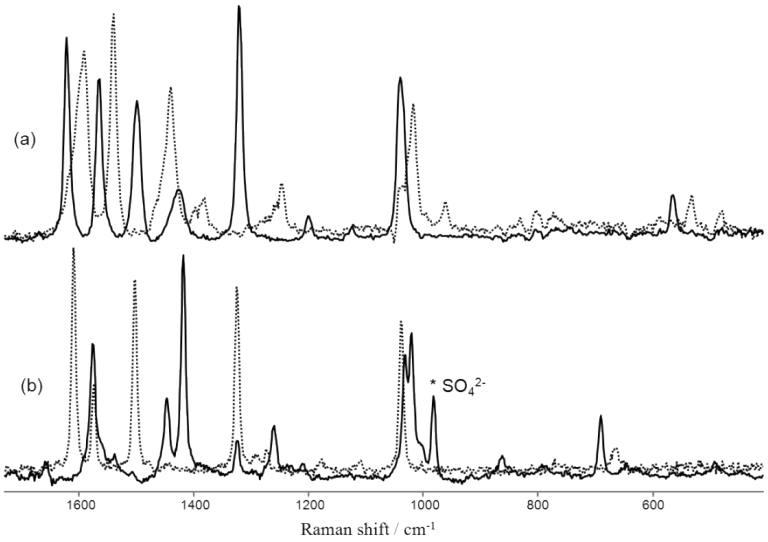

Fig. S 15 Raman spectra of complexes (a) **1** (solid) and **1a** (dotted) (b) **2** (solid) and **2a** (dotted) at 0.3 mM in 20 mM MOPS buffer at λ_{exc} 355 nm. Raman Spectra were solvent subtracted followed by a multipoint baseline correction. * Sulphate band.

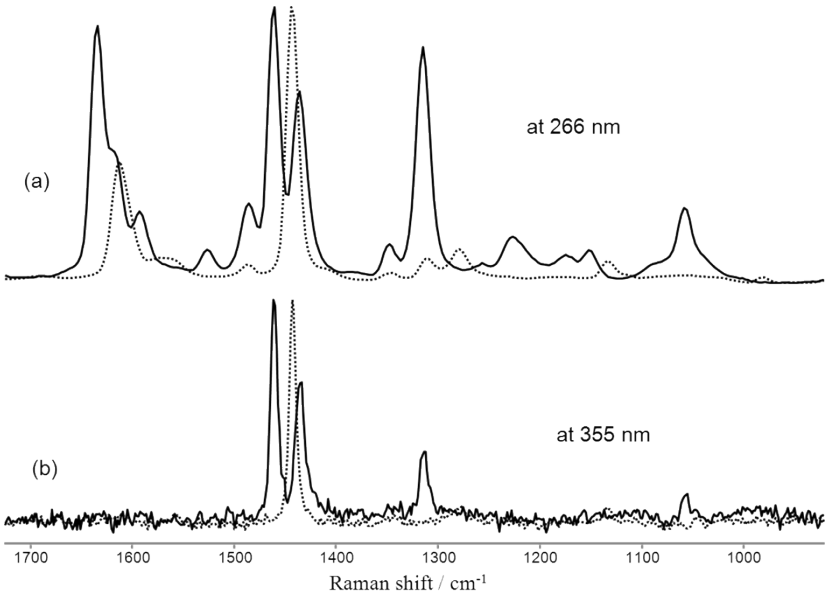

Fig. S 16 Resonance Raman spectra of **3** and **3a** at λ_{exc} (a) 266 nm and (b) 355 nm at 0.3 mM in 20 mM MOPS buffer. Raman spectra were solvent subtracted followed by a multipoint baseline correction.

Raman and resonance Raman spectroscopy

The Raman and resonance Raman spectra of complex **1 - 4** were obtained λ_{exc} at 244, 266, 355, 473 and 785 nm. As expected, the relative intensity of individual bands is strongly excitation

wavelength dependent under conditions where resonant enhancement is achieved, however, in all cases the band positions remain unaltered (Fig. S17-20).

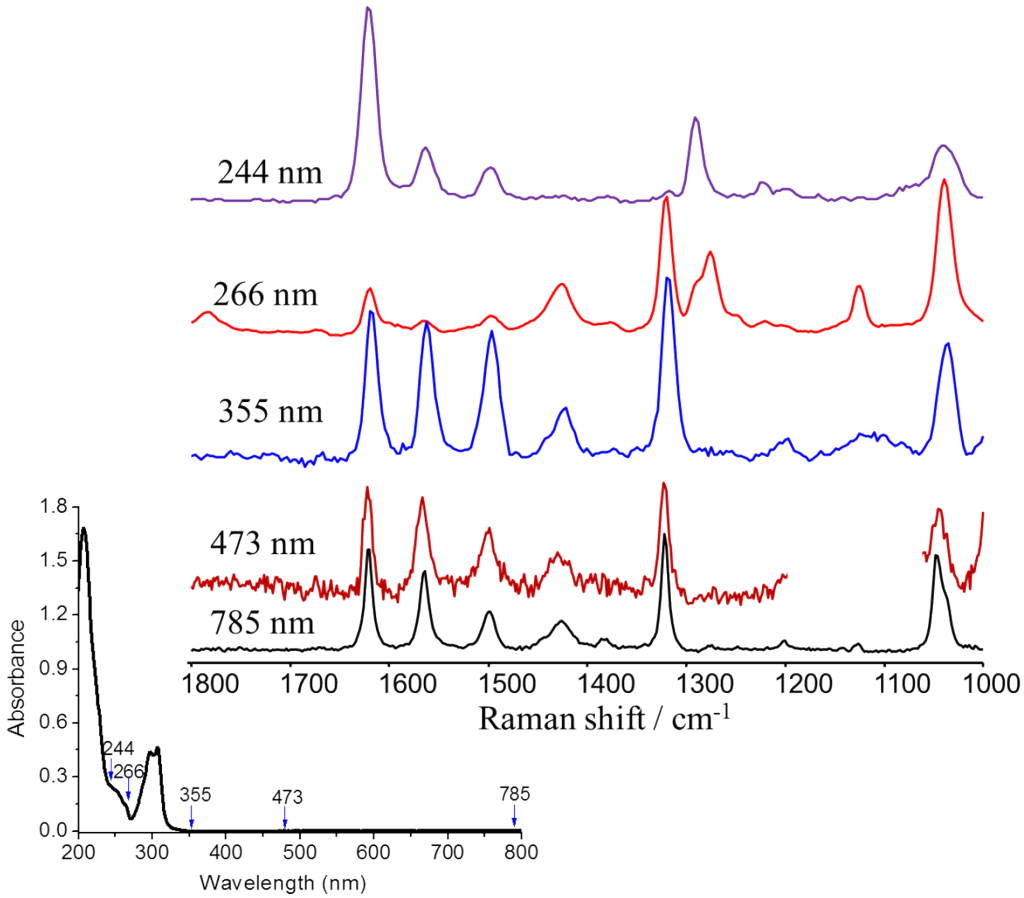

Fig. S 17 UV/Vis absorption (0.03 mM) and wavelength dependent (resonance)Raman spectra of **1** (at 0.3 mM) in 20 mM MOPS buffer at pH 6.5. Raman spectrum obtained at λ_{exc} 785 nm is in water. A spectral artefact is masked by a white box at λ_{exc} 473 nm. Raman spectra are solvent subtracted and a multipoint baseline correction has been applied.

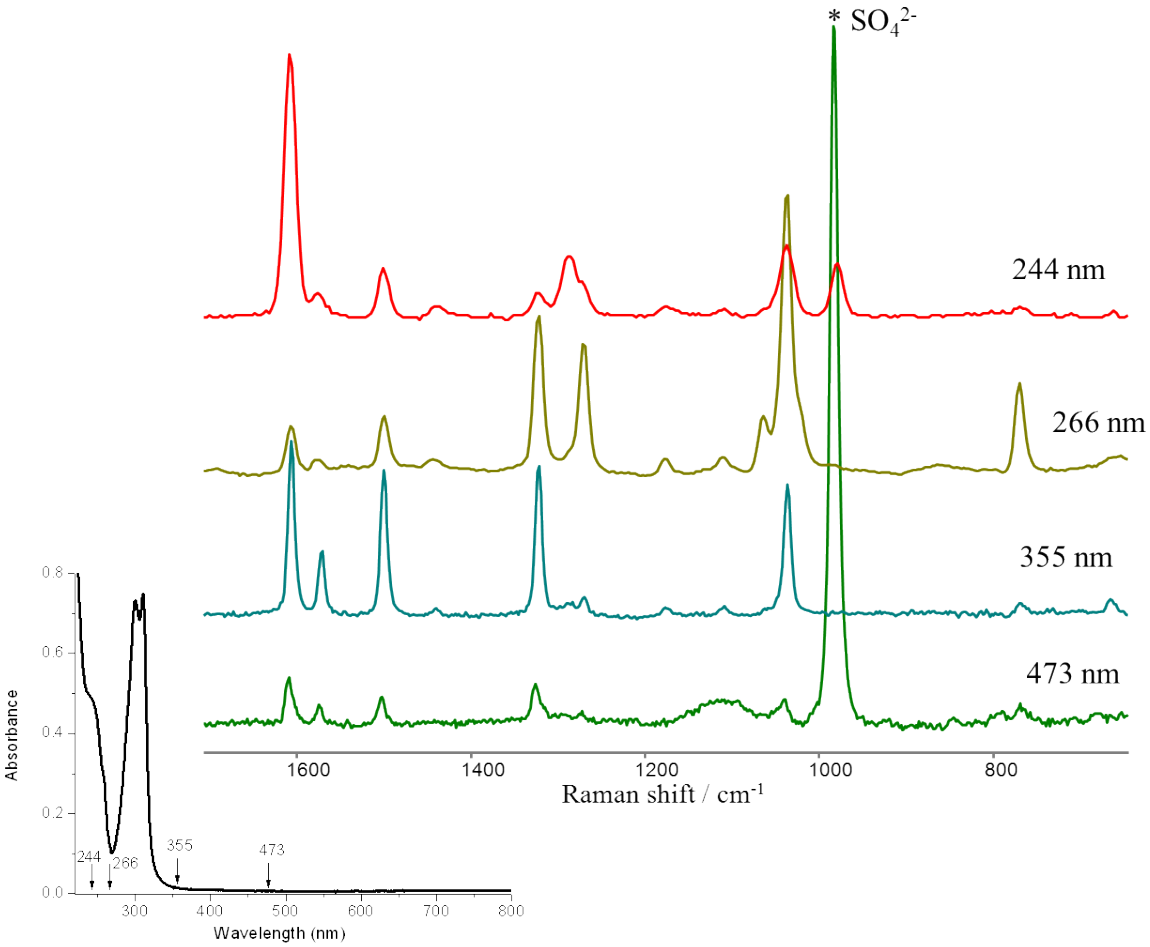

Fig. S 18 UV/Vis absorption (0.03 mM) and wavelength dependent (resonance)Raman spectra of **2** (at 0.3 mM) in 20 mM MOPS buffer at pH 6.5. Raman Spectra were solvent subtracted followed by a multipoint baseline correction.

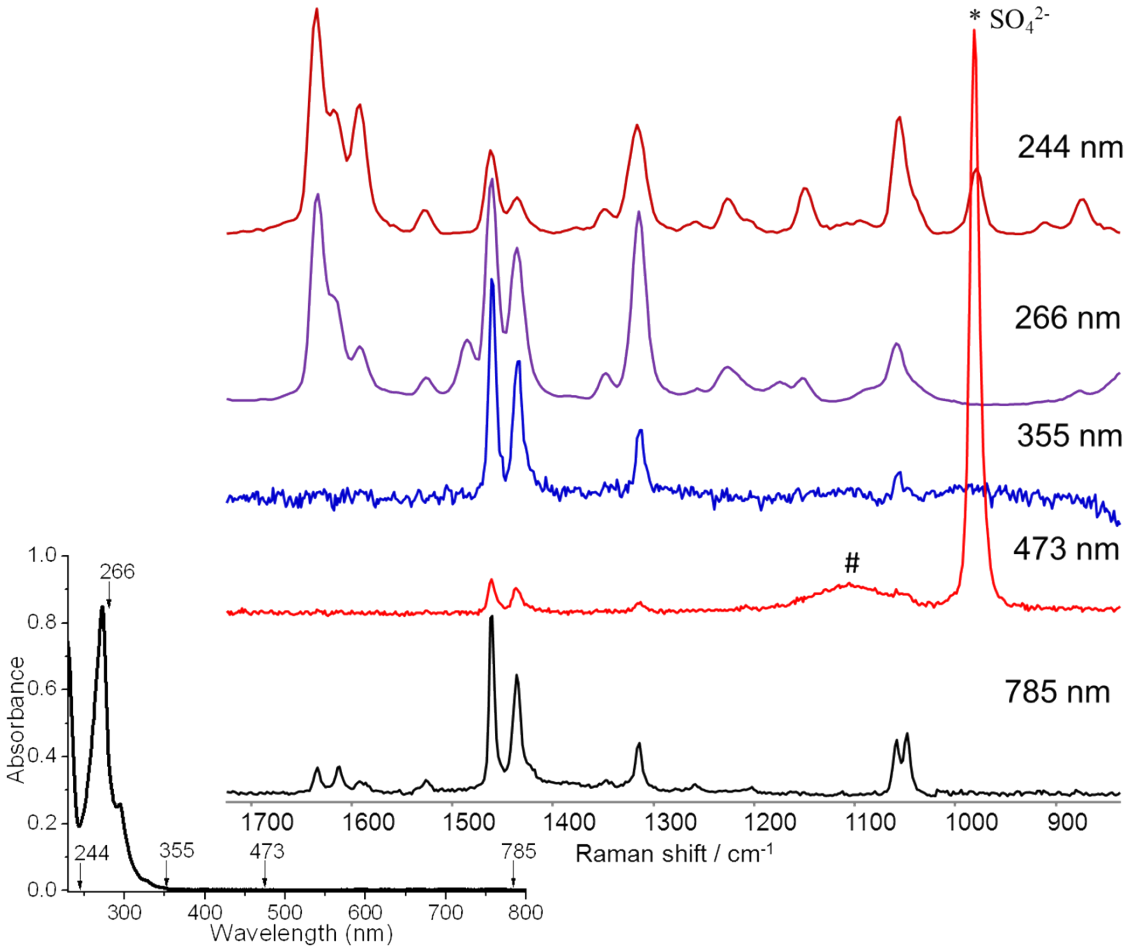

Fig. S 19 UV/Vis absorption (at 0.03 mM) and wavelength dependent (resonance)Raman spectra (at 0.3 mM in 20 mM MOPS buffer at pH 6.5) of **3**. The Raman spectrum obtained at λ_{exc} 785 nm was in water. Raman Spectra were solvent subtracted followed by a multipoint baseline correction. # spectral artifact.

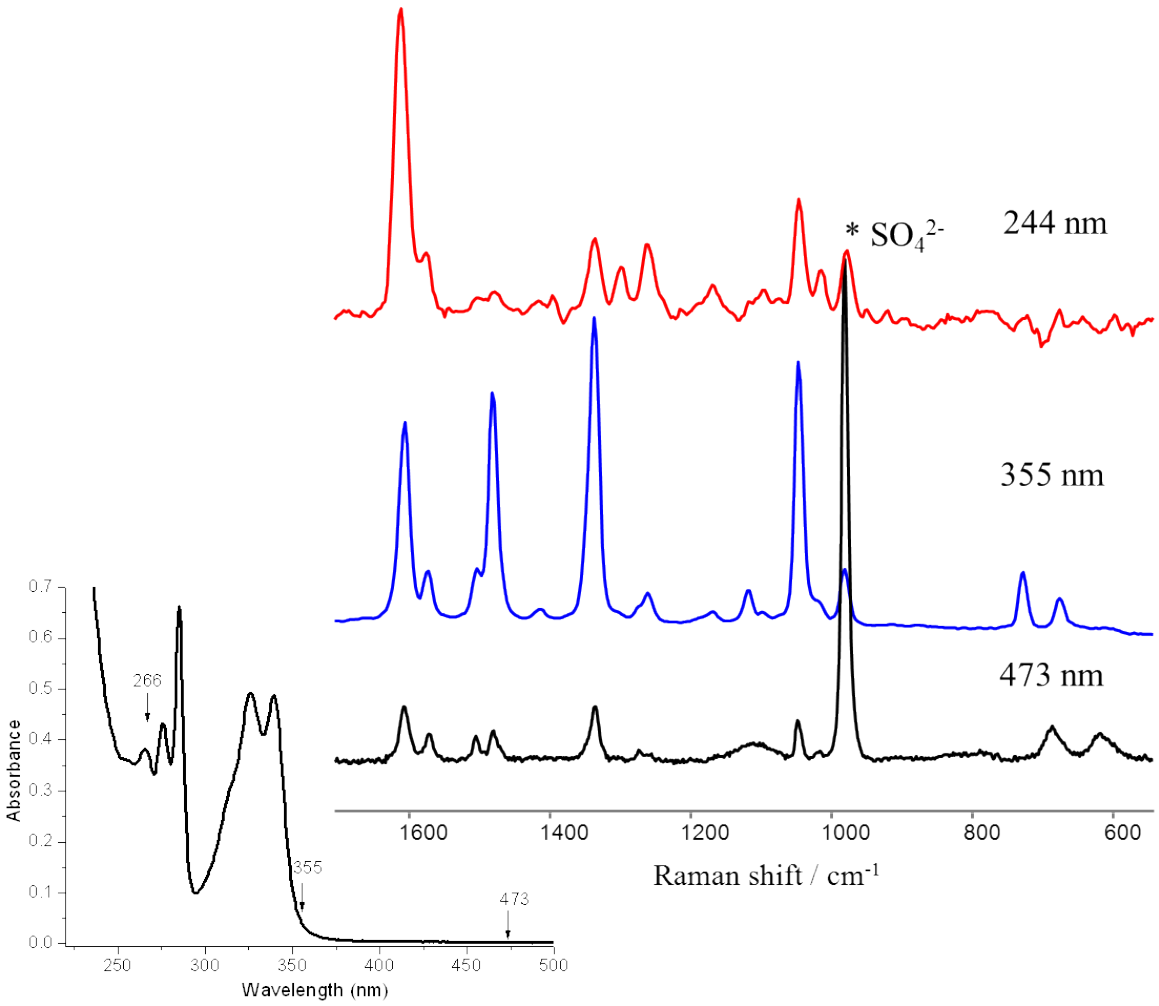

Fig. S 20 UV/Vis absorption (0.03 mM) and wavelength dependent (resonance)Raman spectra of **4** (at 0.3 mM) in 20 mM MOPS buffer at pH 6.5. Raman Spectra were solvent subtracted followed by a multipoint baseline correction.

Complexes **5** and **6** provide relatively rich resonance Raman spectra at λ_{exc} 355 nm and, unsurprisingly given the structural similarity of the ligands dpq and dppz, the spectra of **5** and **6** appear similar, albeit with complex **6** showing additional bands (Fig. S 21).

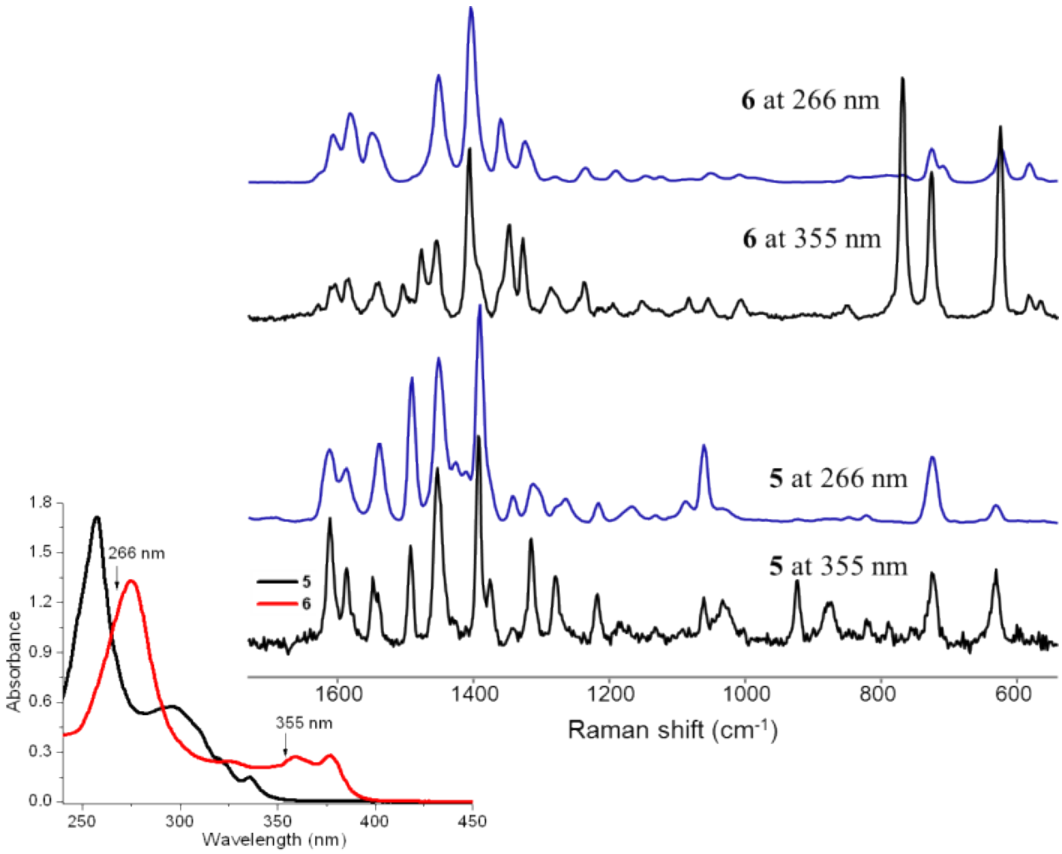

Fig. S 21 UV/Vis absorption (0.03 mM) and wavelength dependent (resonance)Raman spectra of **5** and **6** (at 0.3 mM) in 20 mM MOPS buffer at pH 6.5.

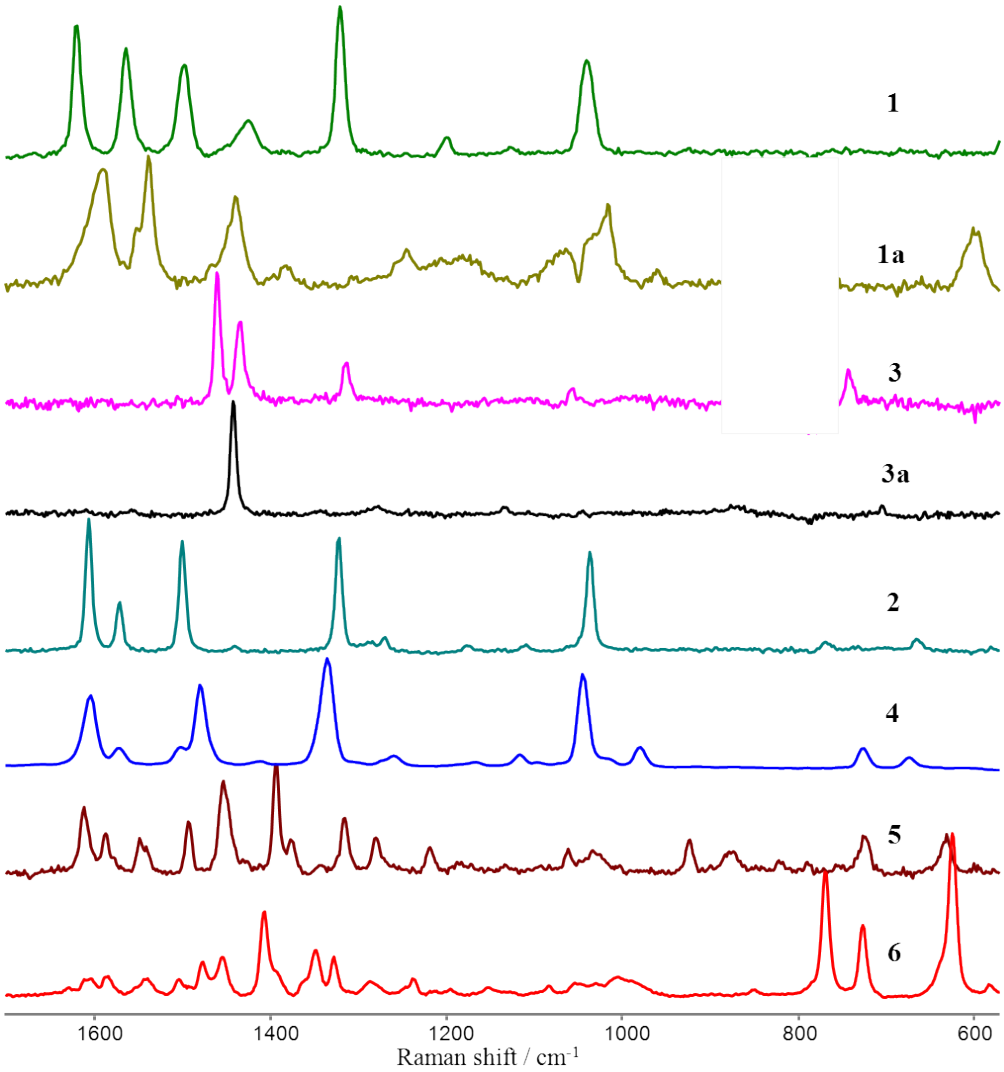

Fig. S 22 Raman spectra of the complexes **1** to **6** are at λ_{exc} 355 nm in 20 mM MOPS at pH 6.5. Raman Spectra were solvent subtracted followed by a multipoint baseline correction. Spectral artifacts are masked with white box.

7. EPR spectroscopy at 77 K

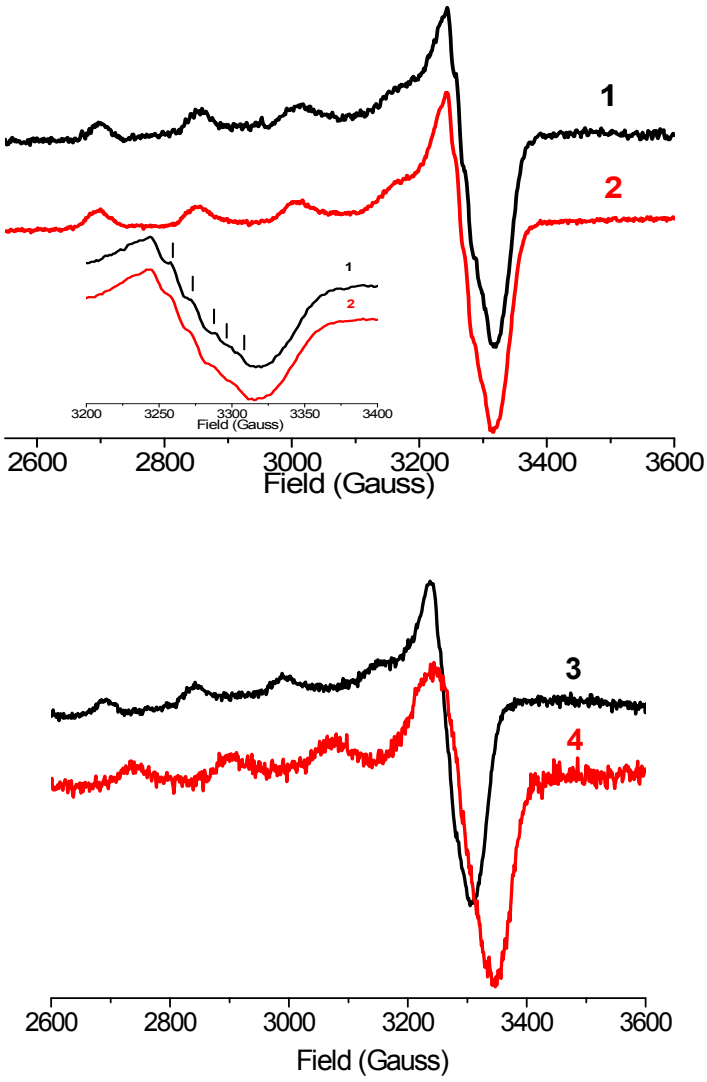

Fig. S 23 X-band EPR spectra of **1** - **4** (0.3 mM) in 20 mM mops at pH 6.5 (1.8 vol% DMSO present to improve glass formation). Experimental conditions: T = 77 K; Microwave frequency = 9.46 GHz; microwave power = 20 mW; 10 G field modulation amplitude; time constant 81.92 ms; conversion time 81.92 ms; 3 accumulations.

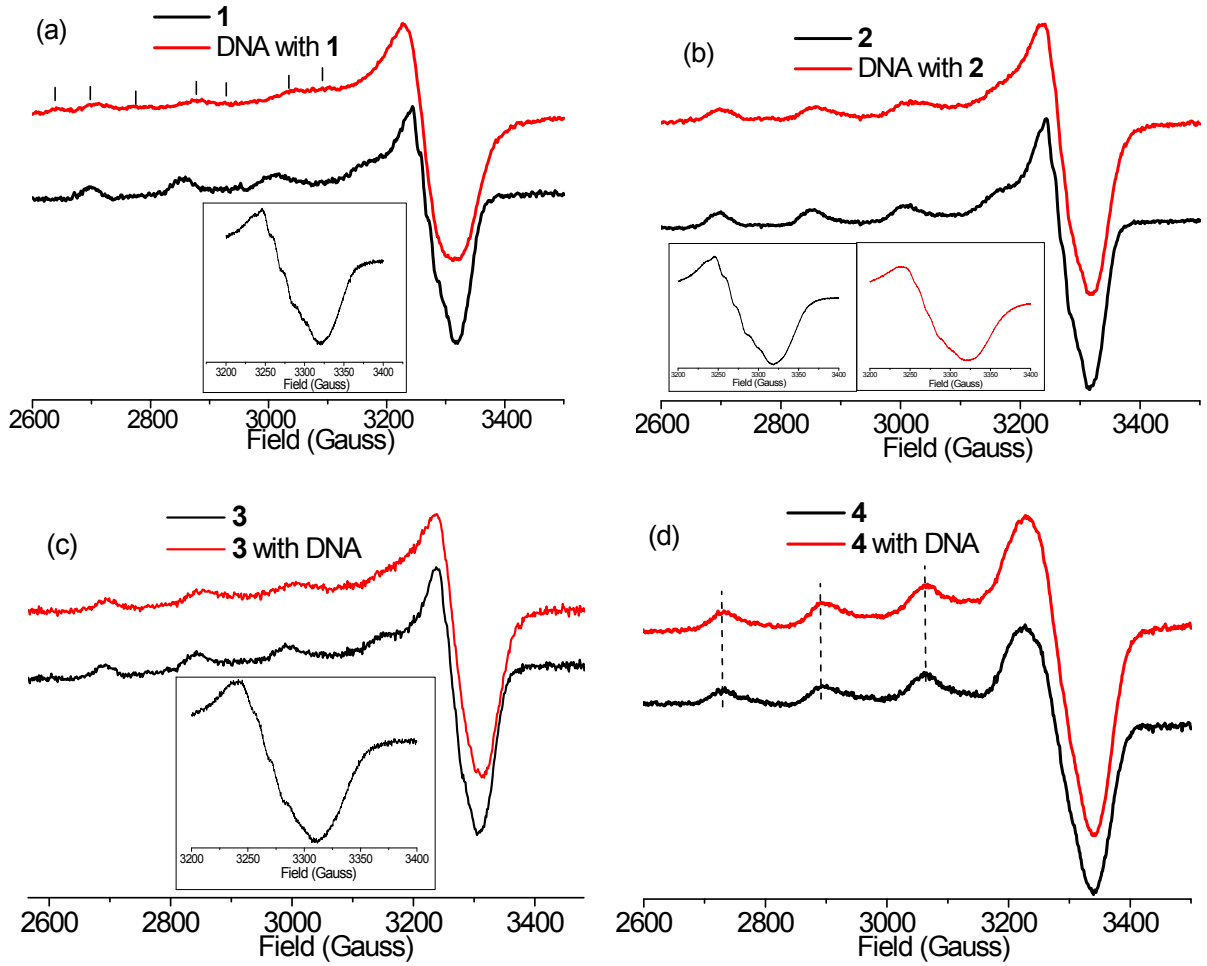

Fig. S 24 EPR spectra of **1** - **4** with and without st-DNA. Conditions: the ratio of the Cu(II) complex to DNA base pairs was 1:6. For (a) st-DNA (2.8 mg/mL), **1** (0.6 mM), (b) st-DNA (1.4 mg/mL), **2** (0.3 mM), (c) st-DNA (1.4 mg/mL), **3** (0.3 mM) and (d) st-DNA (1.4 mg/mL), **4** (0.3 mM) in 20 mM MOPS buffer at pH 6.5 with 1.8 vol% DMSO at 77 K.

8. Room temperature EPR spectroscopy

The EPR spectra were performed initially in frozen solutions, however, as **1** binds st-DNA only weakly, the dynamics of binding might actually be an important parameter in DNA-based catalysis. EPR spectra of **1** recorded in solution at room temperature show the expected isotropic spectrum. However, binding to st-DNA molecule slows the rate of rotation of binding molecules and an anisotropic spectrum can be obtained. The spectra of **1**, **2** and **5** show anisotropicity in the presence of st-DNA (Fig. S25), which is expressed as a change in shape of the spectra towards that of the spectra recorded at 77 K. Unsurprisingly, the effect is most pronounced in the case of **5**, which binds st-DNA strongly via intercalation (Fig. S 25e,f). The observed changes in the shape of the spectra due to the presence of st-DNA in the case of **1** and **2** are similar to **5** (Fig. S 25a-d).

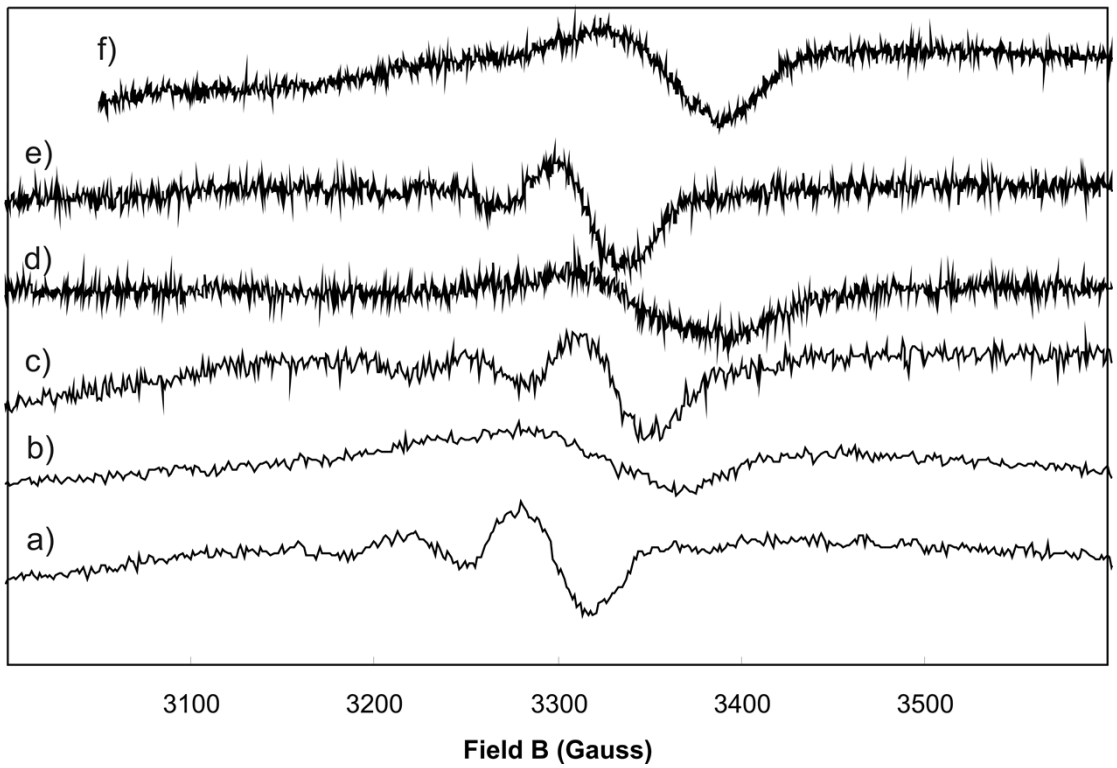

Fig. S 25 X-band EPR at room temperature in 20 mM MOPS at pH 6.5. Experimental conditions: T = 293 K; Microwave frequency = 9.77 GHz; microwave power = 0.2 mW; 1.0 G field modulation amplitude; time constant 20.48 ms; scan time 167.77 s; 6 accumulations. a) 0.6 mM **1** b) 0.6 mM **1**, 2.8 mg/mL st-DNA, c) 0.3 mM **2**, d) 0.3 mM **2**, 1.4 mg/mL st-DNA, e) 0.3 mM **5**, f) 0.3 mM **5**, 1.4 mg/mL st-DNA.

9. Effect of ionic strength

Increasing the ionic strength decreases the affinity of the copper(II) complexes for st-DNA, and it was expected that upon addition of salt the signals of unbound **1** would reappear. However, in the presence of 50 mM NaCl the spectrum of **1**/DNA showed a spectrum similar to what was observed with the oligonucleotides (Fig. S26-28). The changes possibly arise from coordination of the chloride anion to copper, since the affinity of chloride anion in water to copper(II) can be high ($pK_1 = 4$, $pK_2 = 4.7$, $pK_3 = 1.6$, $pK_4 = 0.17$). In order to proof this, a less coordinating anion such as NO_3^- at the same ionic strength should be tested.

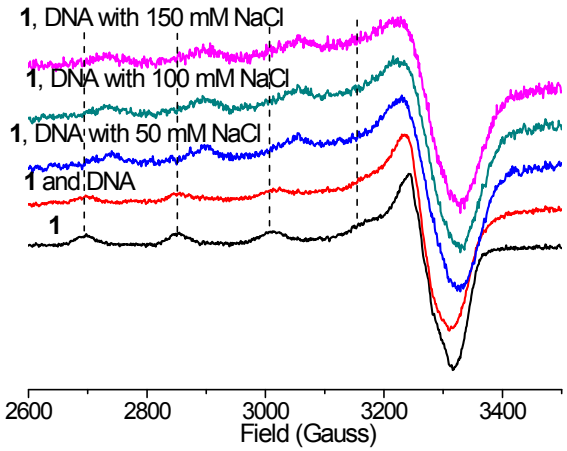

Fig. S 26 Effect of NaCl on binding affinity of **1** with st-DNA. Conditions: ratio of the Cu(II) complex to base pairs DNA is 1:6. st-DNA (1.4 mg/mL), **1** (0.3 mM) in 20 mM MOPS buffer at pH 6.5 with 1.8 vol% DMSO at 77 K. Concentration of NaCl varied from 50 to 150 mM.

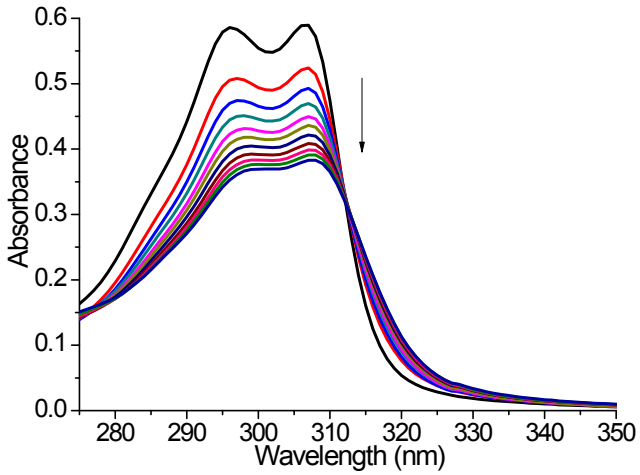

Fig. S 27 Titration of 0.03 mM **1** in increments of 0.01 mM in base pairs of st-DNA in 20 mM MOPS pH 6.5 monitored by UV/Vis absorption spectroscopy. Contributions of the DNA to the absorption spectrum are subtracted.

10. Sequence dependent EPR spectroscopy

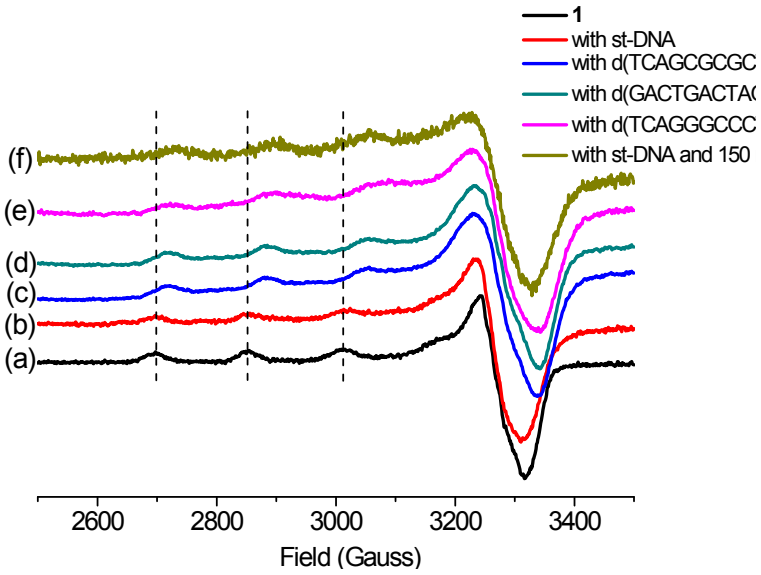

Fig. S 28 X-band EPR of **1** in buffer (20 mM MOPS at pH 6.5, 1.8 vol% DMSO), and in the presence of DNA. Experimental conditions: T = 77 K; Microwave frequency = 9.46 GHz; microwave power = 20 mW; 10 G field modulation amplitude; time constant 81.92 ms; scan time 83.89 s; 3 accumulations. 9 accumulations in the case of c – e. a) 0.3 mM **1**, b) 0.3 mM **1** and 1.4 mg/mL st-DNA, c) 0.25 mM **1**, 1.2 mg/mL $d(TCAGCGCGCTGA)_2$, d) 0.25 mM **1**, 1.2 mg/mL $d(GACTGACTAGTCAGTC)_2$, e) 0.25 mM **1**, 1.2 mg/mL $d(TCAGGGCCCTGA)_2$ and (f) 0.3 mM **1** and 1.4 mg/mL st-DNA and 150 mM NaCl.

11. UV/Vis absorption spectroscopy

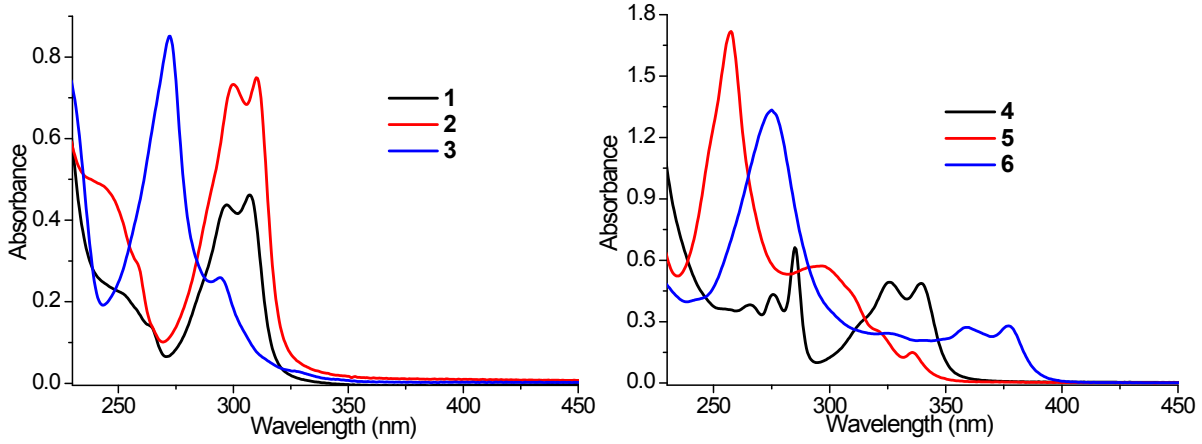

Fig. S 29 UV/Vis absorption spectra of complexes **1** to **6** (0.03 mM) in Milli-Q water. In the case of **5** and **6** 0.03 vol% of DMSO was present.

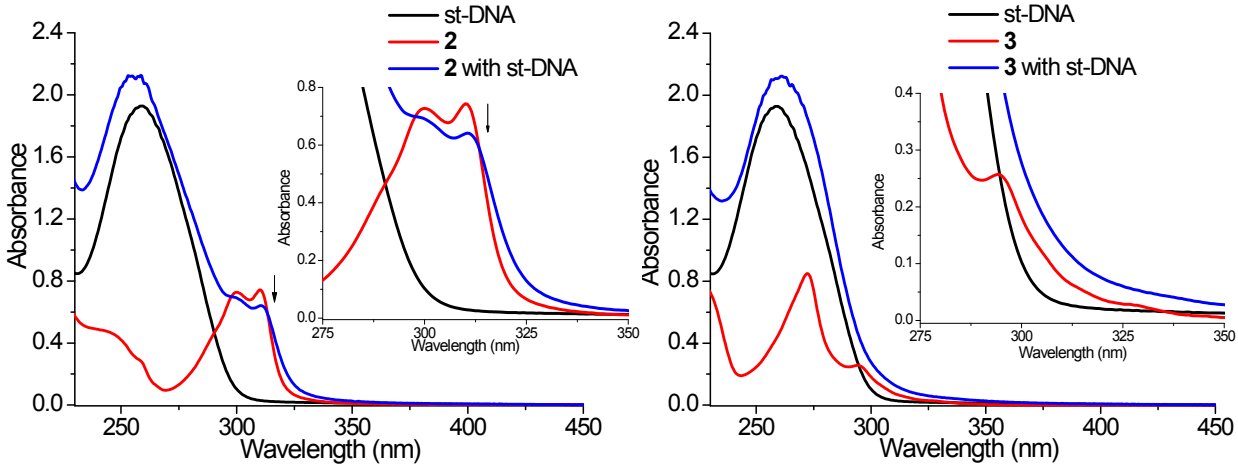

Fig. S 30 UV/Vis absorption spectra of complexes **2** and **3** (0.03 mM) in the absence and presence of st-DNA (0.13 mg/mL). The ratio of the copper complex to DNA base pairs is 1:6.

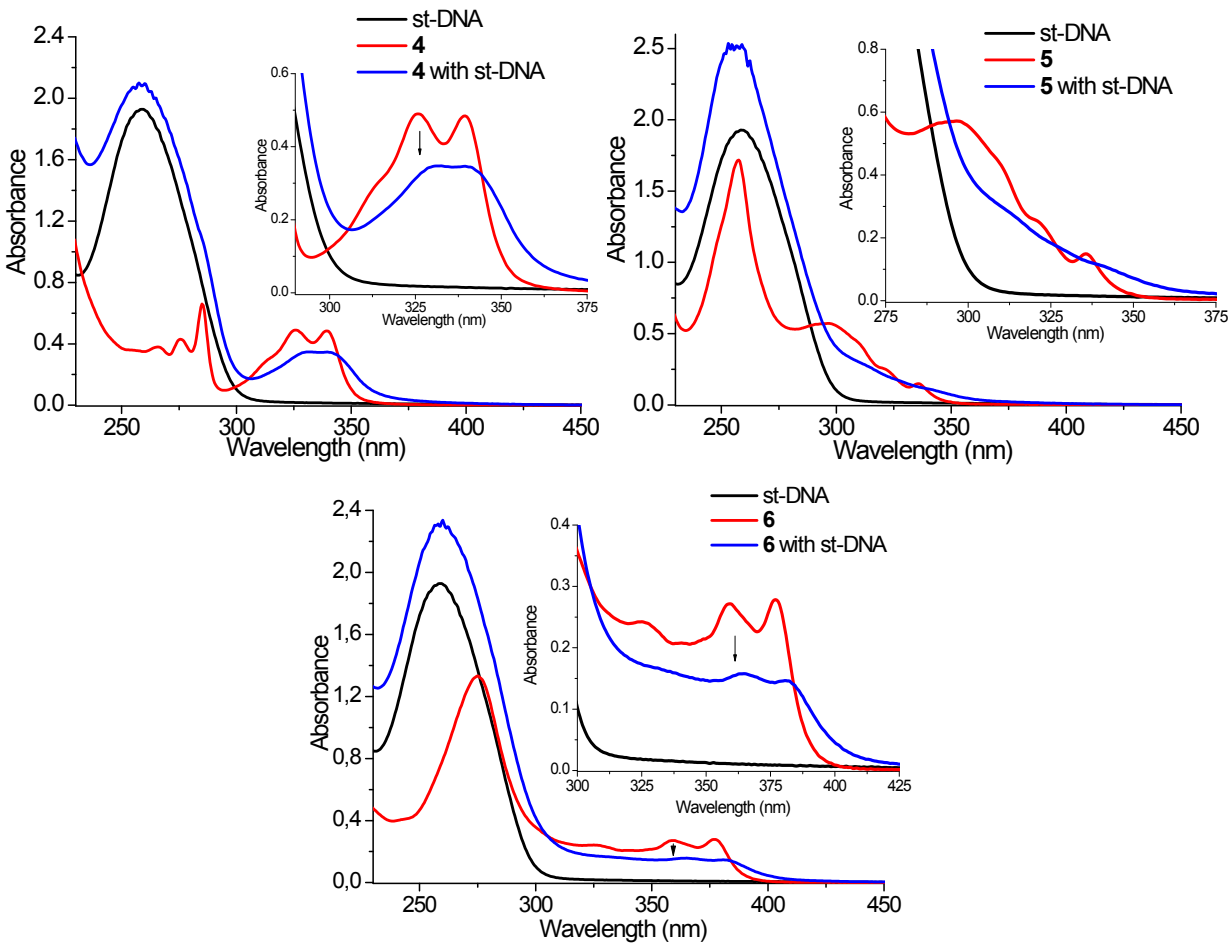

Fig. S 31 UV/Vis absorption spectra of complexes **4**, **5** and **6** (0.03 mM) in the absence and presence of st-DNA (0.13 mg/mL). The ratio of the copper complex to DNA base pairs is 1:6. With 0.03 vol% of DMSO in the case of **5** and **6**.

12. Interaction of Cu-L with st-DNA (Raman and resonance Raman spectroscopy)

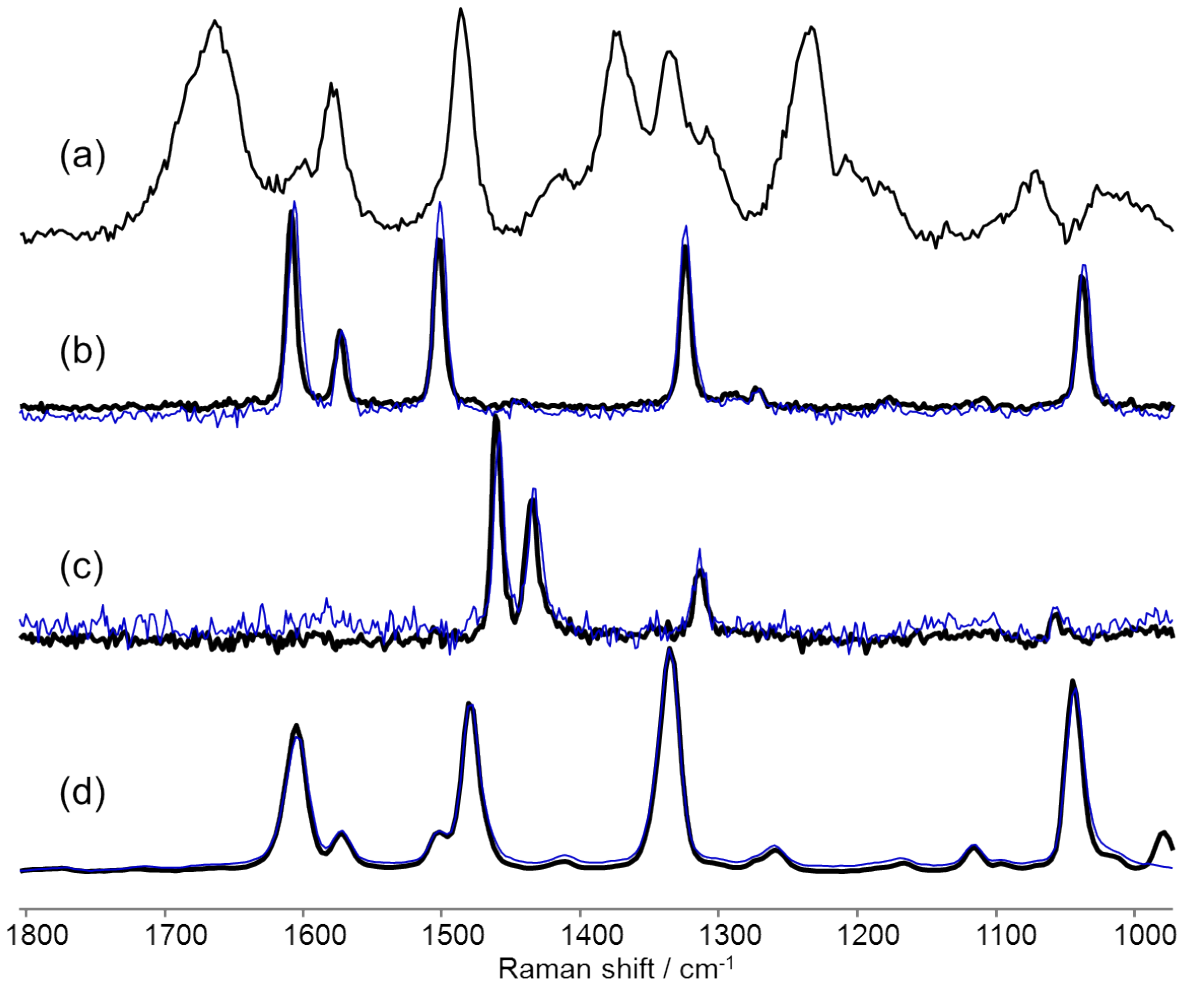

Fig. S 32 Raman spectra of the complexes (b) **2**, (c) **3** and (d) **4** in the presence (thin blue line) and absence of st-DNA (thick solid line) are at λ_{exc} 355 nm. Raman Spectra were solvent subtracted followed by a multipoint baseline correction (contributions from st-DNA were subtracted).

13. Effect of salts on the Raman, EPR and UV/Vis absorption spectroscopy of 1 and 5

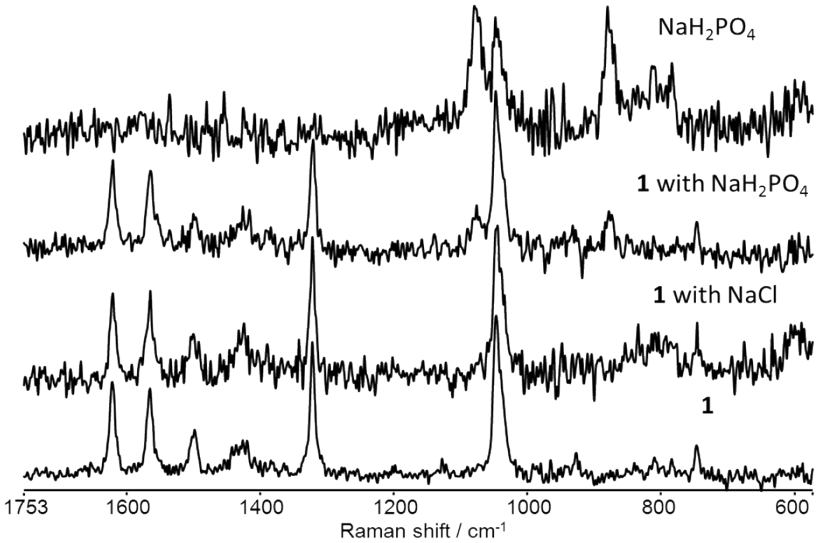

Fig. S 33 Raman spectra of **1**, **1** with NaCl, **1** with NaH_2PO_4 and NaH_2PO_4 in MOPS at λ_{exc} 785 nm. Conditions: **1** (20 mM), NaCl (150 mM) and NaH_2PO_4 (100 mM). Raman Spectra were solvent subtracted followed by a multipoint baseline correction.

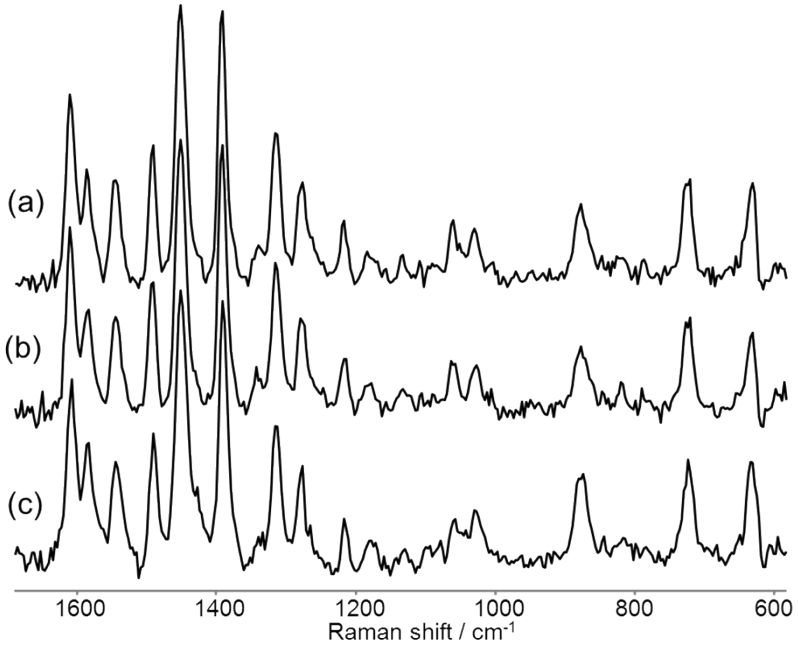

Fig. S 34 Resonance Raman spectra of (a) **5** (b) **5** with NaCl and (c) **5** with NaH_2PO_4 in MOPS with 0.4 vol% D_6-DMSO at λ_{exc} 355 nm. Conditions: **5** (0.3 mM), NaCl (150 mM) and NaH_2PO_4 (150 mM). Raman Spectra were solvent subtracted followed by a multipoint baseline correction.

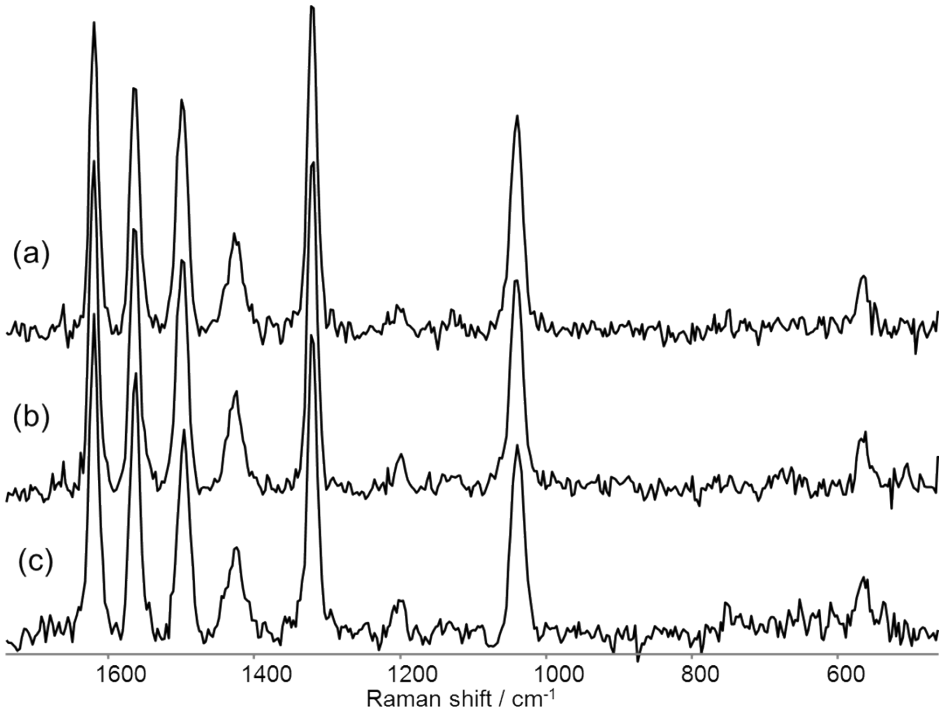

Fig. S 35 Resonance Raman spectra of (a) **1** (b) **1** with NaCl and (c) **1** with NaH_2PO_4 in MOPS at λ_{exc} 355 nm. Conditions: **1** (0.3 mM), NaCl (150 mM) and NaH_2PO_4 (150 mM). Raman Spectra were solvent subtracted followed by a multipoint baseline correction.

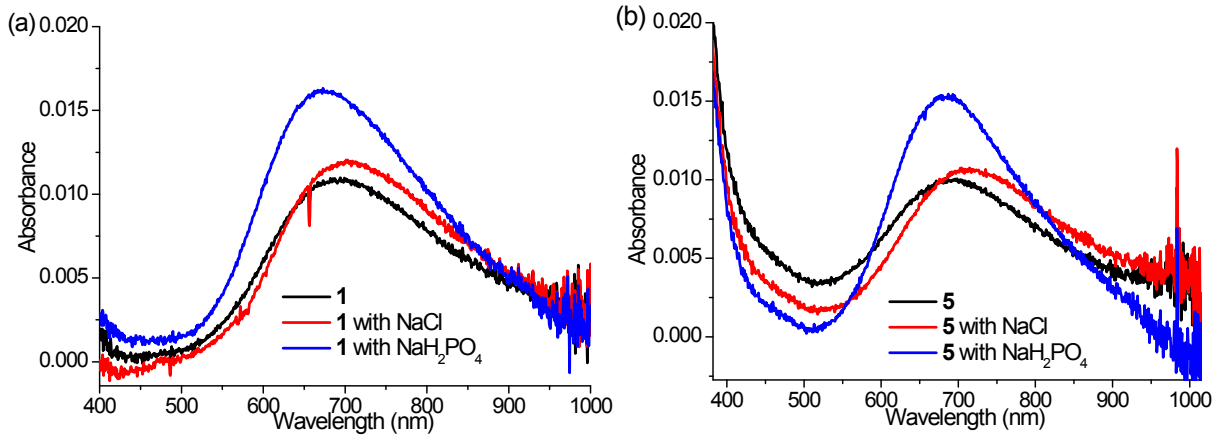

Fig. S 36 UV/Vis absorption spectra of (a) **1**, **1** with NaCl and **1** with NaH_2PO_4 in MOPS with 0.4 vol% d_6-DMSO and (b) **5**, **5** with NaCl and **5** with NaH_2PO_4 in 20 mM MOPS at pH 6.5. Conditions: **1** and **5** (0.3 mM), NaCl (150 mM) and NaH_2PO_4 (150 mM).

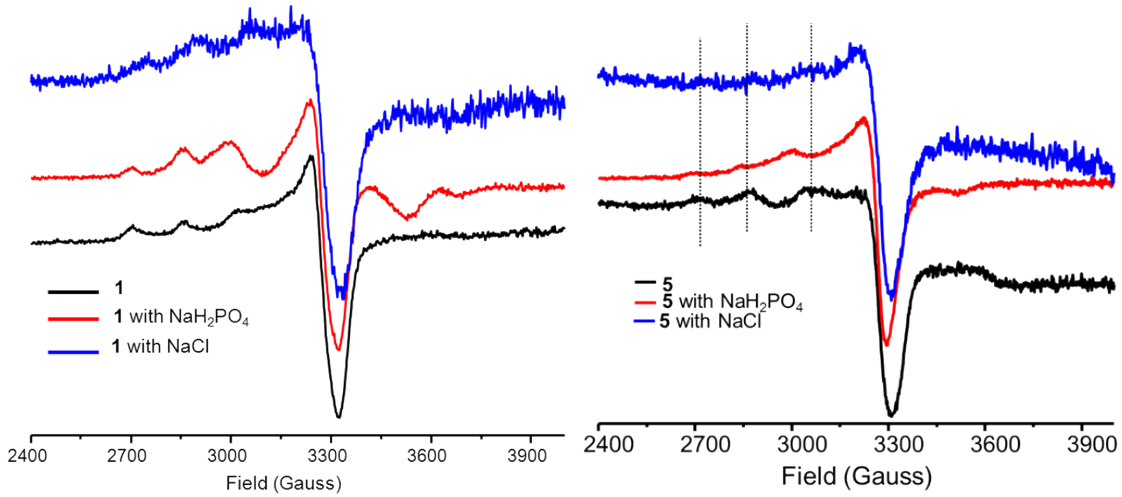

Fig. S 37 EPR spectra of (left) **1**, **1** with NaCl and **1** with NaH_2PO_4 and (right) **5**, **5** with NaCl and **5** with NaH_2PO_4 in MOPS with 1.8 vol% DMSO. Conditions: **1** and **5** (0.3 mM), NaCl (150 mM) and NaH_2PO_4 (150 mM). Experimental conditions: T = 77 K; Microwave frequency = 9.46 GHz; microwave power = 63.5 mW; 10 G field modulation amplitude; time constant 81.92 ms; conversion time 81.92 s; 3 accumulations. EPR spectra were background subtracted.

14. Circular Dichroism

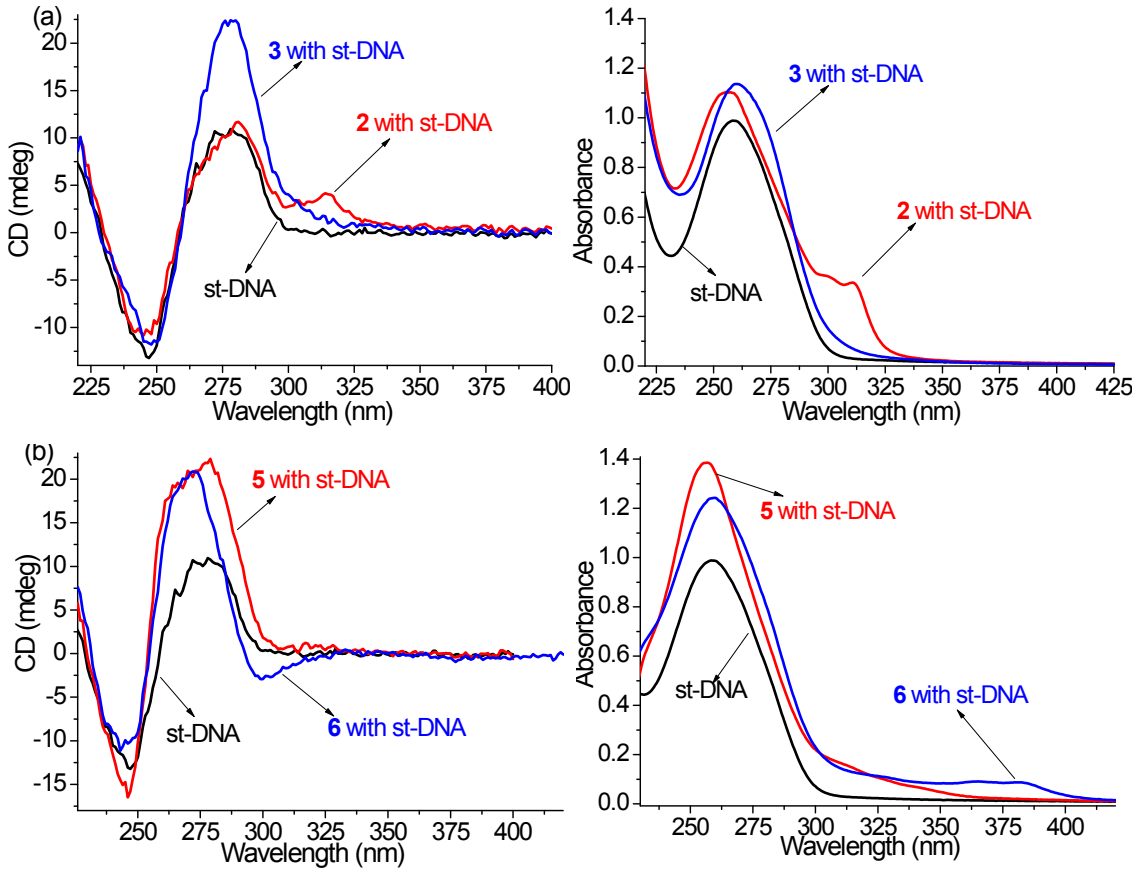

Fig. 38 CD and UV/Vis absorption spectra of **2**, **3**, **5** and **6** in the presence of st-DNA (a and b). Conditions: ratio of the Cu complex to DNA base pairs is 1:6. st-DNA (0.065 mg/mL), Cu complex (0.015 mM) in Milli-Q water.

14. Linear Dichroism

The reduced LD (LD^r) was calculated from:

$$LD^r(\lambda) = \frac{LD(\lambda)}{A_{iso}(\lambda)}$$

where A_{iso} is the isotropic absorbance. The angle (α) between the transition moment of the absorption band of the Cu(II) complex and the axis of the DNA helix was related to the LD^r according to:

$$LD^r = \frac{3}{2} S3\left(\left(\cos^2 \alpha\right) - 1\right)$$

where S is the orientation parameter. The orientation parameter was determined by assuming the angle (α) between the macroscopic orientation axis and the transition moment to be 86°.

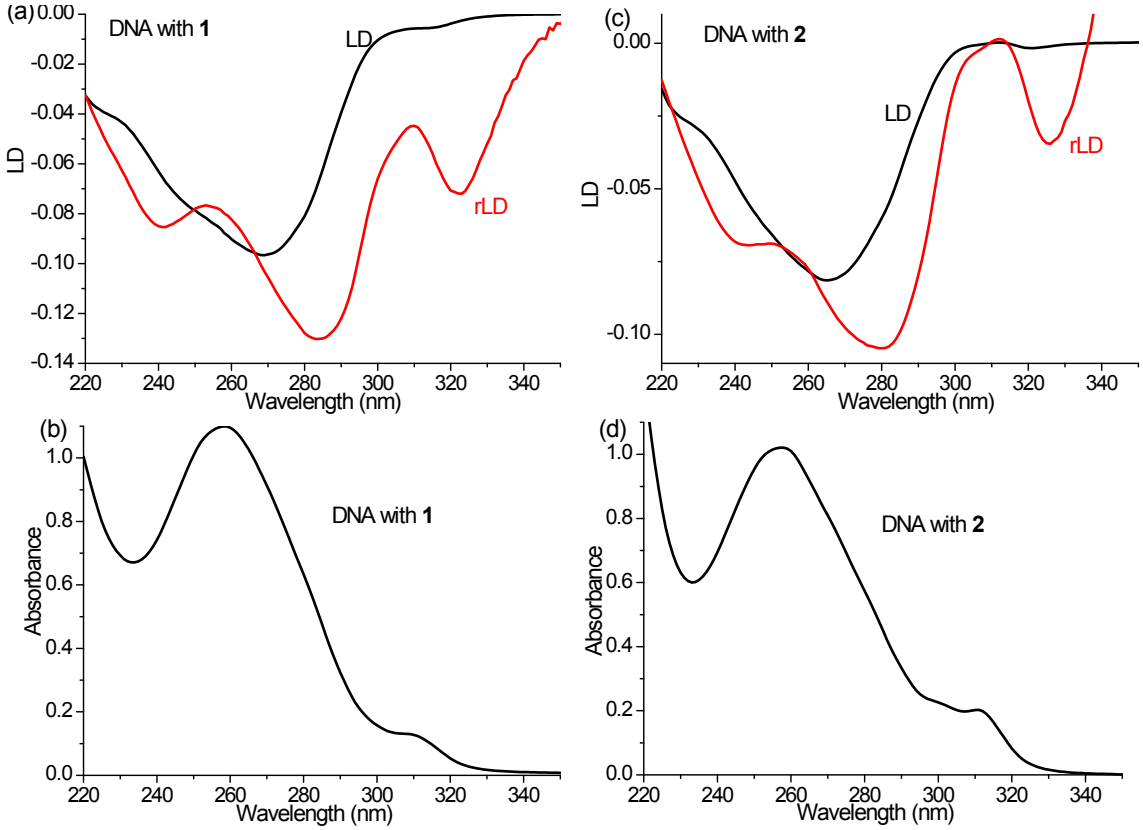

Fig. S 39 LD, rLD and isotropic absorption spectra in the presence of st-DNA of **1** (a and b) and **2** (c and d) (at 0.3 mM) and st-DNA (1.4 mg/mL) in MOPS 20 mM at pH 6.5.

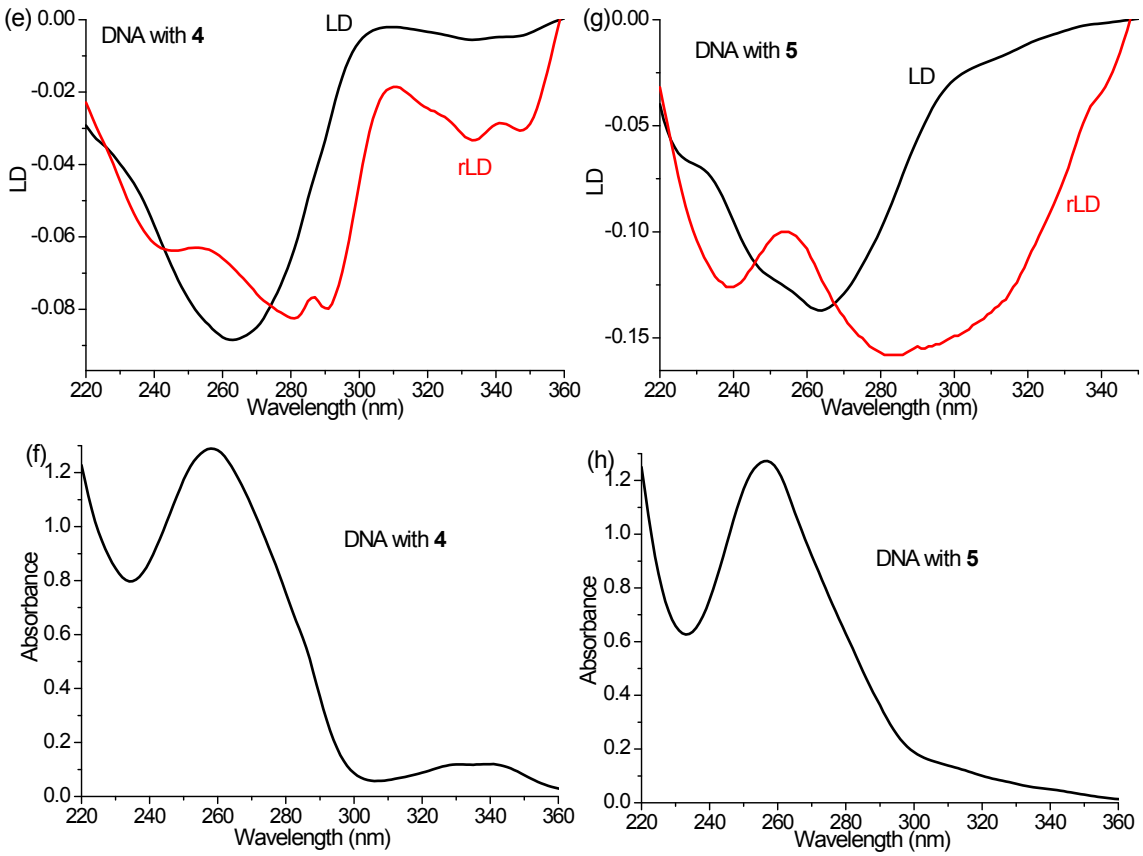

Fig. S 40 LD, rLD and isotropic absorption spectra in the presence of st-DNA of **4** (e and f) and **5** (g and h) (at 0.3 mM) and st-DNA (1.4 mg/mL) in MOPS 20 mM at pH 6.5.

15. Viscosity

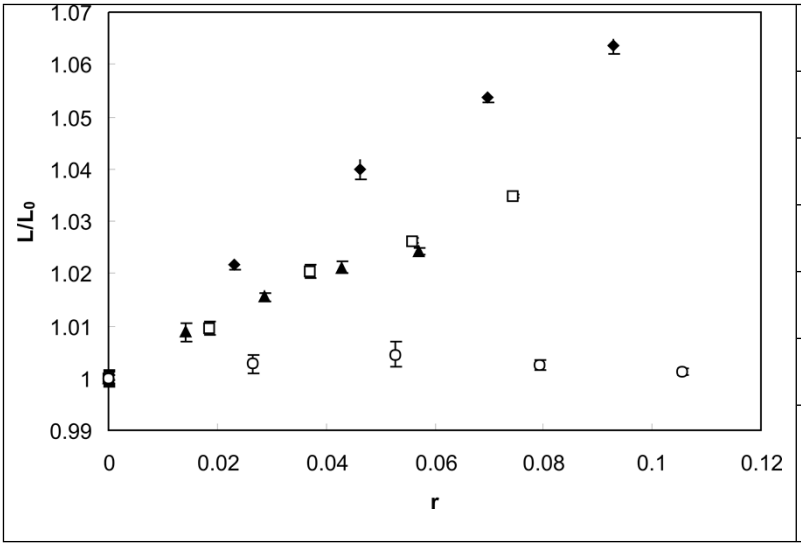

	Slope
1	0.322
2	0.278
3	0.609
4	0.592
5	0.641
Hoechst 33258	0.049

Fig. S 41 Titration of **1** - **5** to st-DNA followed by the viscometry. (i) **1** (open squares), (ii) **2** (triangles), (iii) **4** (diamonds) and (iv) Hoechst 33258 (open circles), in 20 mM MOPS buffer, pH 6.5, at 22.0 °C. L/L_0 is the apparent length of the st-DNA, r is the ratio [Cu-L]:[DNA base pairs].

References

1 W. R. Browne, C. M. O'Connor, J. S. Killeen, A. L. Guckian, M. Burke, P. James, M. Burke and J. G. Vos, *Inorg. Chem.,* 2002, **41**, 4245.

2 A. Draksharapu, Q. Li, H. Logtenberg, T. A. van den Berg, A. Meetsma, J. S. Killeen, B. L. Feringa, R. Hage, G. Roelfes and W. R. Browne, *Inorg. Chem.*, 2012, **51**, 900.

3 http://www.kromatek.co.uk/categories/Linear-Dichroism-Couettes/ on 20140904.

4 F. Menges, "Spekwin32 - optical spectroscopy software", Version 1.71.6.1, 2012, ttp://www.effemm2.de/spekwin/

5 ASTM E1840-96(2007) Standard Guide for Raman Shift Standards for Spectrometer Calibration, ASTM International, **DOI:** 10.1520/E1840-96R07.

6 G. Cohen and H. K. Eisenberg, *Biopolymers,* 1969, **8**, 45.

7 G. Roelfes, A. J. Boersma and B. L. Feringa, *Chem. Commun.* 2006, 635.

8 H. E. Gottlieb, V. Kotlyar and A. Nudelman, *J. Org. Chem.*, 1997, **62**, 7512.

9 (a) Z. Q. Wen and G. J., Thomas, Jr., *Biopolymers*, 1998, **45**, 247; (b) M. C. Tobin, *Spectrochimica Acta*., 1969, **25A**, 1855.

10 K. M. Knee, S. B. Dixit, C. E. Aitken, S. Ponomarev, D. L. Beveridge and I. Mukerji, *Biophysical J.,* 2008, **95**, 257.

11 S. P. Sinha, *Spectrochim. Acta*., 1964, **20**, 879.

12 (a) B. M. Gatehouse, S. E. Livingstone and R. S. Nyholm, *J. Inorg. Nucl. Chem.*, 1958, **8**, 75; (b) D. E. Irish and A. R. Davis, *Can. J. Chem.*, 1968, **46**, 943.

13 A. R. Davis and C. Chong, *Inorg. Chem.*, 1972, **11**, 1891.